Energy & Buildings 255 (2022) 111666

Contents lists available at ScienceDirect

Energy & Buildings

journal homepage: www.elsevier.com/locate/enb

Feasibility of MOF-based carbon capture from indoor spaces as air revitalization system

Jean Paul Harrouz [a], Kamel Ghali [a], Mohamad Hmadeh [b], Nesreen Ghaddar [a,*], Saud Ghani [c]

[a] Department of Mechanical Engineering, American University of Beirut, Beirut 1107 2020, Lebanon
[b] Department of Chemistry, American University of Beirut, Beirut 1107 2020, Lebanon
[c] Department of Mechanical and Industrial Engineering, College of Engineering, Qatar University, P.O. Box: 2713, Doha, Qatar

ARTICLE INFO

Article history:
Received 19 August 2021
Revised 17 October 2021
Accepted 8 November 2021
Available online 13 November 2021

Keywords:
Carbon capture
Solid desiccant
Sustainable ventilation system
Metal organic frameworks
Indoor air quality

ABSTRACT

Conventional air-conditioning systems, for providing thermal comfort and acceptable indoor air quality, are energy intensive, especially for spaces located in hot and humid climates. This is attributed to the energy needed to offset the latent and sensible loads of the ambient air, which is typically achieved using a solid desiccant integrated with a vapor compression cooling. Air revitalization system (ARS) is proposed as an alternative solution to remove excess H_2O and CO_2 sequentially from the recirculated air using solid adsorbents such as silica gel for H_2O and metal–organic frameworks (MOFs) for CO_2. In this work, the feasibility of MOFs-based ARS is investigated by predicting its operational performance cost and compare it to the conventional system. Accordingly, mathematical models were developed for the adsorption beds and the indoor space and integrated to genetic algorithm. The integrated model was used to properly size and optimize the system for a classroom and a residential house located in the Qatari climate. The simulation results showed that the ARS decreased the fresh air intake by 91% and 71%, for the classroom and house, respectively, leading to savings of 30% and 24% as well as payback periods of 5 and 2 years compared to the conventional system.

1. Introduction

Nowadays, it has become a global trend for people to conduct the majority of their activities in indoor spaces [1]. As a consequence, it is essential to ensure acceptable indoor environmental quality to protect people health and well-being [2,3]. This is achieved by regulating the indoor temperature and relative humidity (RH) to maintain acceptable levels of thermal comfort and by diluting the indoor contaminants' concentration levels (e.g., CO_2, VOCs, particulate matter) to acceptable limits for good indoor air quality (IAQ) [4]. Concentrations exceeding certain thresholds can have effects ranging from compromising occupants' cognitive performance to causing diseases and bodily dysfunctions [5–8]. To reduce these concentrations to acceptable levels, large quantities of ambient clean air are needed. However, the ambient air must be conditioned (humidified/dehumidified, heated/cooled) before being supplied, to ensure occupants' thermal comfort needs. For that purpose, heating, ventilation and air-conditioning (HVAC) systems have been widely used during high load seasons [9,10]. Conventional HVAC systems are based on vapor compression cooling either as standalone systems or integrated with solid desiccant (e.g. silica gel) to dehumidify and cool the needed quantities of ambient fresh air [10]. In the Gulf regions (e.g., Qatar), where extreme hot and humid climates dominate throughout the year, buildings that rely on the traditional HVAC systems consume considerable amounts of energy [11–13]. This is due to the high electric power consumption of the compressor as well as the high thermal energy needed to regenerate the desiccant when it is used [14]. As these systems rely primarily on fossil fuel combustion, the building's carbon emissions increase contributing to global warming, which in turn increases the load for HVAC and energy use [15,16]. Therefore, it is important to seek alternative solutions to reduce the buildings' ventilation and cooling loads without compromising the occupants' thermal comfort and IAQ levels.

In conventional systems, filtered ambient air has been mainly supplied to dilute the indoor CO_2 concentrations, which is the gas recognized by ASHRAE as the surrogate ventilation index. CO_2 concentration level in an air conditioned room is a good indicator of occupancy and ventilation rate within a space [17]. Hence, regulating CO_2 simultaneously keeps other contaminants' concentrations (e.g., VOCs), below their limit levels [18,19]. A novel energy-friendly ventilation strategy that can be used in the extreme Gulf climate, would be carbon capture. This strategy con-

* Corresponding author.
E-mail address: farah@aub.edu.lb (N. Ghaddar).

https://doi.org/10.1016/j.enbuild.2021.111666
0378-7788/

Nomenclature

ARS	*Air Revitalization System*
C_i	*Species concentration in an airstream (kg/m^3)*
CO_2	*Carbon dioxide*
C_p	*Specific heat capacity (J/kg·K)*
D	*Diameter (m)*
ΔH_i	*Heat of adsorption (J/kg)*
D_{zi}	*Axial diffusion coefficient (m^2/s)*
E	*Energy (kW)*
H	*Height (m)*
h_{sg}	*Convective heat transfer coefficient (W/m^2·K)*
HCHO	*Formaldehyde*
HVAC	*Heating, ventilation and air-conditioning*
IAQ	*Indoor air quality*
J	*Objective function (USD)*
k_i	*LDF constant (s^{-1})*
LCC	*Life cycle cost (USD)*
LCCA	*Life cycle cost analysis*
LDF	*Linear driving force*
$\dot{m}$	*Mass flowrate (kg/s)*
MOFs	*Metal-organic frameworks*
O_2	*Dioxygen*
$\overline{q}$	*uptake capacity (kg/kg)*
$\dot{Q}(t)$	*heat source (W)*
RH	*Relative humidity (%)*
S_h	*Horizontal solar radiation (W/m^2)*
t	*Time (s)*
T	*Temperature (°C)*
u	*Interstitial velocity (m/s)*
U_{wg}	*overall heat transfer coefficient (W/m^2·K)*
V	*Volume (m^3)*
VOCs	*Volatile organic compounds*
$\dot{Y}_i$	*Indoor species generation/consumption rate (kg/s)*
y_i	*Species concentration in indoor air (kg/m^3)*
z	*Space coordinate (m)*

Greek symbols

α	*Weighting factor*
β	*Bypass fraction (–)*
ε_t	*Total bed porosity (–)*
λ	*Thermal conductivity (W/m·K)*
μ	*Viscosity (Pa·s)*
ω	*Specific humidity (kg/kg)*
ρ	*Density*
Σ_w	*Outer wall specific heat exchange area (m^2/m^3)*

Subscripts

1	*First spatial node in the bed discretization*
a	*Air*
amb	*Ambient*
b	*Bed*
cs	*Conventional system*
e	*Electrical*
ext	*External*
fa	*Fresh air*
g	*Gas*
in	*Inlet*
int	*Internal*
p	*Particle*
purge	*Purge*
ra	*Return air*
reg	*Regeneration*
s	*Solid*
space	*Space*
supp	*Supply*
t	*Thermal*
ta	*Treated air*

sists of removing the excess CO_2 from the indoor air using adsorption [20]. It can potentially save energy as it enables the use of a fraction or fully recirculated indoor air in the supply vent [21]. This has been especially appealing since the heat of adsorption of CO_2 is lower than that of H_2O, which results in lower regeneration energy [22]. In addition, carbon capture systems reduce the fresh ambient air intake to small amounts dedicated to the regulation of indoor O_2 and VOCs levels within the IAQ constraints, leading to energy savings.

Several researchers studied the feasibility of CO_2 adsorption in buildings in hot and humid climates using different solid adsorbents [23]. Zhao et al. [24] showed that carbon capture from indoor air, using amine-functionalized cellulose, maintains indoor CO_2 levels between 1000 and 5000 ppm. Lee et al. [25] numerically studied an adsorption bed packed with activated carbon that maintained indoor CO_2 levels at 3000 ppm. Other studies also investigated the energy savings' potential of carbon capture. Sinha et al. [26] used the conventional zeolite 13X as an adsorbent in an office located in a humid climate. They reported a 75 % reduction in the ventilation load while the indoor CO_2 levels were kept below 5000 ppm. From these studies [23–26], it is noted that carbon capture did not lower the CO_2 levels below the 1000 ppm threshold as recommended by ASHRAE [17]. This is attributed to the adsorbents themselves, where some cannot capture CO_2 at dilute concentrations (~1000 ppm) usually found in buildings, and where other adsorbents (e.g., zeolites) require high regeneration energy. In addition, carbon capture has been studied as a separate process and not integrated within the complete HVAC system, which includes the dehumidification and cooling processes. Therefore, it is important to find new materials that can still capture CO_2 from the dilute indoor levels (400 – 1000 ppm), and can be incorporated as part of a whole HVAC system.

In the last two decades, new generation of highly porous solid adsorbents have emerged, known as metal–organic frameworks (MOFs) [22]. The most appealing property of MOFs is that they can be custom-synthesized to exhibit high capacity for CO_2 in dilute airstreams [27–30]. Park et al. [29], Mukherjee et al. [27] and Bhatt et al. [31] proposed different MOFs that are suitable for CO_2 capture from indoor air and that showed the ability to meet the IAQ constraint of CO_2 level of 1000 ppm. In addition, MOFs exhibit a heat of adsorption (<1000 kJ/kg) and desorption temperature (<80 °C) that are considerably lower than their conventional counterparts (such as zeolites with heat of adsorption of 1136 – 2273 kJ/kg and desorption temperature higher than 150 °C) [32,33]. Therefore, the feasibility of carbon capture becomes even more prominent with MOFs. However, as in the case of the majority of adsorbents, MOFs' affinity to CO_2 is degraded in the presence of humidity due to the higher adsorption selectivity of H_2O over CO_2 [34]. Consequently, the recirculated air must be dehumidified before the carbon capture stage [34]. Additionally, the heat gained by the treated air due to the release of heat of adsorption from H_2O and CO_2 increases the needed cooling energy. Therefore, a feasibility study of indoor carbon capture is needed, where the HVAC system's total energy consumption is assessed, including: electrical energy for the dehumidification and carbon capture, thermal energy for the regeneration of the beds, as well as the electrical

energy of the vapor compression air-conditioner. As a hybrid system is considered, the number of operating parameters increase, which turns this feasibility study into an optimization problem that aims to minimize operating costs while meeting the recommended thermal comfort and IAQ constraints of the space.

To the authors' knowledge, no other study has investigated the optimized performance of the complete HVAC system relying on carbon capture from indoor air using MOFs. For this reason, a hybrid system, known as the air revitalization system (ARS) is proposed that integrates two packed beds in series to remove excess H_2O and CO_2 from the room air, followed by a vapor compression air-conditioning system. The dehumidification can be carried out using a conventional desiccant such as silica gel characterized by its low cost and low regeneration temperature (<80 °C) [35]. For carbon capture, a commercially available MOF-74-Mg is selected as a suitable adsorbent for this application [36]. It has been studied for carbon capture from the ambient air (CO_2 level of 400 ppm) and was found to exhibit an uptake capacity of 6.3 g/kg and does not require an airstream to be excessively dry for effective CO_2 adsorption [30]. In addition, MOF-74-Mg presented a low heat of adsorption of 954 kJ/kg, along with a regeneration temperature of 60 °C [37]. The ARS energy performance is then compared to that of the conventional system that dehumidifies and cools ambient air using a silica gel packed bed and a vapor compression air-conditioning, respectively.

The development of a sustainable HVAC is highly needed since such a system is capable of reducing fresh ambient air amounts in hot humid climates while meeting the indoor air quality requirements (acceptable levels of indoor humidity, CO_2, VOCs and O_2). In densely occupied spaces, such a system can then considerably reduce the building energy consumption. For this reason, it is crucial to study the feasibility of the complete HVAC system incorporating the ARS while determining its optimal operational parameters for best performance. Therefore, to minimize the systems operating cost without compromising the occupants' thermal comfort and IAQ levels, the operating parameters of both proposed ARS and conventional systems must be optimized on an hourly basis as a function of the ambient and indoor conditions. Accordingly, a mathematical model is developed for the heat and mass transfers in the silica gel and MOFs adsorption packed beds. The model is then validated against published data and used to properly size the adsorption beds of both systems. The model is used to determine the optimal performance of each system using the genetic algorithm. This is achieved for two case studies of low (residential house) and high (classroom) occupancy density buildings, located in the predominantly hot and humid Qatari climate that is characterized by large variations in its ambient conditions. These case studies tend to highlight the advantages of the ARS over the conventional system at different ambient and indoor conditions. Finally, a life cycle cost analysis (LCCA) is finally conducted to determine the ARS payback period if it was retrofitted within buildings HVAC system.

2. System description

In this work, two typical air-tight Qatari buildings are considered with two different occupancy densities: a residential house representative of low occupancy buildings and a classroom representative of high occupancy buildings. Clean conditioned air is supplied to the spaces to obtain the indoor design thermal comfort and IAQ constraints. The occupants' thermal comfort is met by regulating the indoor temperatures between 22 °C and 24 °C and indoor RH between 40% and 65% [38]. The CO_2 levels should be maintained below 1000 ppm [39], whereas O_2 levels should be kept above 195,000 ppm (or 19.5 % in volume) [40]. In addition, the indoor formaldehyde (one of the most commonly found VOCs in indoor spaces) levels should be kept below 0.08 ppm [41–43]. To achieve these requirements, two HVAC systems can be used: i) the conventional system consisting of a packed adsorption bed to dehumidify the ambient air (Fig. 1(a)), or ii) the ARS consisting of two packed adsorption beds to remove excess H_2O and CO_2 form the room return air and to minimize the fresh ambient air requirement (Fig. 1(b)). Due to the batch nature of adsorption processes, each system has two adsorption beds that are operated out-of-phase for the dehumidification and carbon capture. During adsorption, the beds are cooled by promoting ambient air movement around them [25], while during regeneration, a hot air stream is passed in the beds to heat the adsorbent and purge the desorbed adsorbate (H_2O and CO_2).

For the conventional system, the adsorption bed is packed with silica gel (type RD) to dehumidify a fraction (β_{CS}) of the ambient air ($\dot{m}_{fa,CS}$) at state (1), where β_{CS} is adjusted as function of the ambient conditions to control the humidity of the supply air. To reduce the cooling load of the vapor compressor air-conditioner, a sensible heat recovery heat exchanger is installed between the exhausted room air (heated from state (2) to (7)) and the airstream leaving the packed bed is cooled from state (3) to (4) (see Fig. 1a). The air at state (4) is then mixed with the bypassed air as well as the fraction $\dot{m}_{ra,CS}$ of the recirculated air in a mixing box. The resulting air mixture ($\dot{m}_{supp}$) at state (5) is sensibly cooled to state (6) in the air-conditioner. The different ventilation air state points in the conventional system are presented on a psychrometric chart in Fig. 1 (a).

Using the proposed ARS, a sequential operation of desiccant dehumidification and carbon capture is shown in Fig. 1(b). The flowrate ($\dot{m}_{fa,ARS}$) of ambient fresh air at state (1) is needed to regulate the O_2 and formaldehyde levels within the IAQ set-points. Only a fraction ($\dot{m}_{ta,ARS}$) of the room air needs to be treated in the adsorption beds to maintain the space IAQ recommended levels and is regulated as a function of the obtained supply conditions. Due to the high selectivity of H_2O over CO_2 in the MOFs, the recirculated air at state (2) is passed into the silica gel packed bed in order to reduce the air humidity at state (3) to 4 g/kg [27], avoiding thus the degradation of MOF-74-Mg capacity for CO_2. The dehumidified hot air is then sensible cooled to state (4) with the exhausted room air that is discharged at state (8). This is crucial to decrease the adsorption temperature in the MOFs bed and maintain the adsorbent capacity for CO_2. The CO_2-depleted air at state (5) is later mixed with the fractions $\dot{m}_{ra,ARS}$ and $\dot{m}_{fa,ARS}$ of recirculated air and ambient air, respectively. The air mixture ($\dot{m}_{supp}$) at state (6) is sensibly cooled in the vapor compression air-conditioner and supplied to the space at state (7). The psychrometric process of the ventilation air treatment using the proposed ARS is shown in Fig. 1(b). It should be noted that for the conventional system, CO_2 is chosen as the surrogate for IAQ control, where the regulation of $\dot{m}_{fa,CS}$ ensures a comprehensive adherence for the broad set of IAQ. On the other hand, for the ARS, the control of CO_2 and water vapor is done using the adsorption system (i.e. $\dot{m}_{ta,ARS}$), whereas that of the other species, formaldehyde and O_2 are chosen as the new surrogates for IAQ and the control of $\dot{m}_{fa,ARS}$ .At each hour, and depending on the varying ambient and indoor conditions, the supply conditions are regulated on an hourly basis to meet the thermal comfort and IAQ requirements. For this reason, the typical vapor compression air-conditioning is operated with constant supply temperature while varying $\dot{m}_{supp}$ to ensure that the space load is met, and the occupants' thermal comfort is achieved. Since this flowrate is a mixture of ambient and recirculated air streams, their fractions are regulated to provide the needed species concentrations in the supply airstream and consequently to meet the spaces' IAQ constraints. Accordingly, the oper-

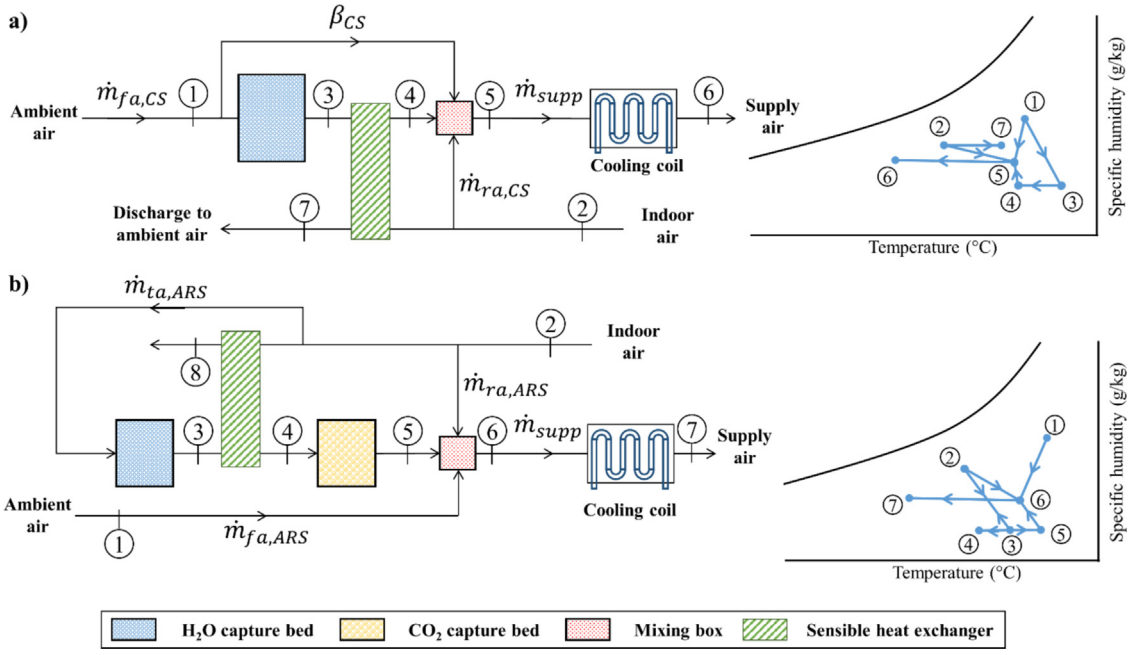

Fig. 1. Schematic of a) conventional system and b) ARS integrated with vapor compression based cooling coil, with the corresponding psychrometric processes.

ating conditions of the conventional system ($\dot{m}_{fa,CS}$ and β_{cs}) and the ARS ($\dot{m}_{fa,ARS}$ and $\dot{m}_{ta,ARS}$) are optimized to enable the two HVAC systems to meet the indoor space constraints at minimal operating cost consisting of the electrical energy to drive the packed adsorption beds' fans and the air-conditioner compressor, as well as the thermal energy required to regenerate the different adsorbents.

3. Methodology

The objective of this work is to assess the performance of the ARS over the entire Qatari hot season and compare it to that of the conventional system. The simulation of both systems require the modeling of the adsorption beds as well as the indoor air conditions. Therefore, a mathematical model is developed to predict the heat and mass transfer inside the adsorption beds to determine the supply conditions. The supply conditions are used as input to a space model that expresses the indoor conditions as function of the building envelope and indoor occupancy. The integrated model of the cooling system and space is used to properly size the different packed beds of both systems and determine their optimal operating parameters that maintain the required thermal comfort and IAQ levels at minimal total operating cost.

3.1. Adsorption bed model

An adsorption bed is used to selectively remove either H_2O or CO_2 from an airstream to regulate the supply conditions and meet the required IAQ levels. The adsorbents, in the form of beads of diameter (D_p), are loosely packed in the adsorption beds of diameter (D_b) and height (H_b) as shown in Fig. 2(a). For the control volume shown in Fig. 2(b), a transient one-dimensional model is developed to predict the coupled mass and heat balances occurring between the gas and solid phases inside the bed [33,44,45]. Since the adsorbed species, H_2O and CO_2, are at dilute levels, the associated loss in mass due to adsorption is negligible compared to the total mass flowrate [44]. Therefore, the mass loss does not affect the fluid velocity, which can be assumed constant across the bed length with an axially dispersed plug flow [46,47]. Furthermore, Ergun's equation is used to estimate the pressure drop across the packed bed [48]. In order to predict the species, H_2O and CO_2, concentration at the bed outlet, the species mass balance is used as follows [33,44]:

$$\frac{\partial C_i}{\partial t} + u\frac{\partial C_i}{\partial z} - D_{zi}\frac{\partial^2 C_i}{\partial z^2} + \left(\frac{1-\varepsilon_t}{\varepsilon_t}\right)\rho_s\frac{\partial \overline{q}_i}{\partial t} = 0 \quad (1)$$

The first term of the equation indicates the unsteady transport. The second and third terms express the total mass flux due convection and diffusion respectively. The last term represents the adsorption into the solid particles. The different parameters in equation (1) represent the following: C_i (kg/m^3) and $\frac{\partial \overline{q}_i}{\partial t}$ (kg/kg·s) are the concentration and the average adsorption rate of species "i" (H_2O or CO_2) in the gas phase, u (m/s) is the interstitial flow velocity, ρ_s (kg/m^3) and ρ_a (kg/m^3) are the particle and air density, respectively. ε_t (–) is the total porosity that depends on the sorbent porosity as well as the packing density [49]. D_{zi} (m^2/s) is the axial diffusion coefficient given by Wen and Fan correlation [50] and it depends on the flow Reynold and Schmidt numbers and the bed porosity.

The adsorption rate $\left(\frac{\partial \overline{q}_i}{\partial t}\right)$ describes the adsorption kinetics, which have been evaluated using different models with varying degrees of accuracy and computational complexity [33]. The linear driving force (LDF) model has been widely used, since it offers a good compromise between results' accuracy and computational cost. It combines the three mass transfer resistances into a single adsorption rate constant k_i (s^{-1}) [46,48]. Using the LDF model, $\frac{\partial \overline{q}_i}{\partial t}$ of species "i" is proportional to the difference between its equilibrium concentration $\overline{q}_i^*$ (kg/kg) and the volume-averaged adsorbed concentration $\overline{q}_i$ (kg/kg) [33,44]. $\frac{\partial \overline{q}_i}{\partial t}$ is thus given by:

$$\frac{\partial \overline{q}_i}{\partial t} = k_i(\overline{q}_i^* - \overline{q}_i) \quad (2)$$

The concentration $\overline{q}_i^*$ is evaluated from the equilibrium isotherms of the adsorbent-adsorbate pair. It varies with the species concentration C_i determined from equation (1) as well as the adsorbent temperature, which is detemined from the energy equa-

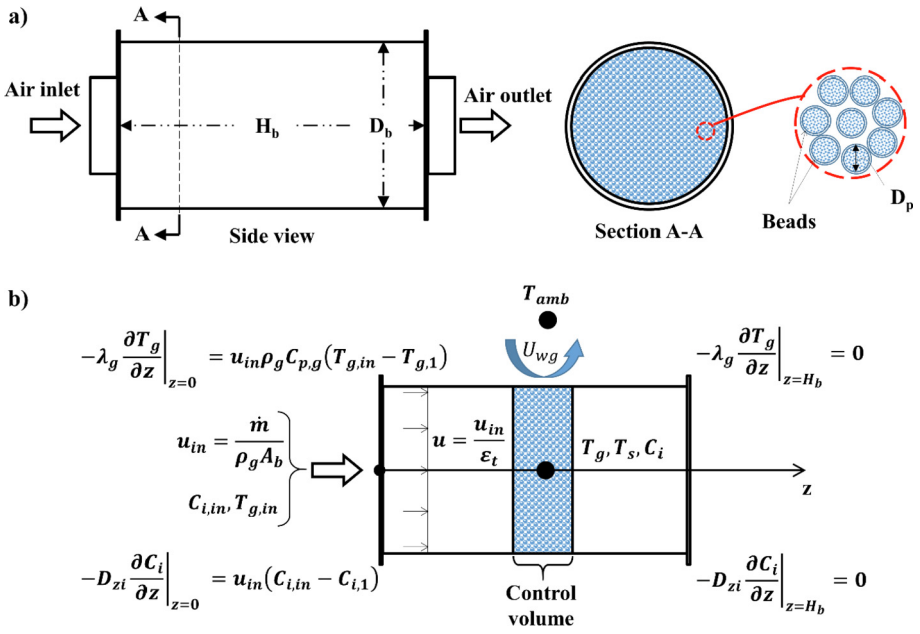

Fig. 2. Schematic of the adopted a) adsorption beds' geometry and b) control volume of the numerical model.

tion of the solid phase. The gas phase energy balance is also needed since local thermal non equilibrium is assumed to enable the precise modeling of the early cycle stages [51]. The solid and gas energy equations are given by [44,52,53]:

$$\rho_s C_{p,s}\frac{\partial T_s}{\partial t} = \lambda_s \frac{\partial^2 T_s}{\partial z^2} + \frac{6h_{sg}}{D_p}(T_g - T_s) + \frac{\rho_s \Delta H_i}{1-\varepsilon_t}\frac{\partial \overline{q}_i}{\partial t} \tag{3}$$

$$\varepsilon_t \rho_g C_{p,g}\left(\frac{\partial T_g}{\partial t} + u\frac{\partial T_g}{\partial z}\right) = \varepsilon_t \lambda_g \frac{\partial^2 T_g}{\partial z^2} + \frac{6h_{sg}}{D_p}(T_s - T_g) + U_{wg}\Sigma_w(T_{amb} - T_g) \tag{4}$$

The left-hand side of equation (3) represents transient storage in the adsorbent, whilst the terms on the right-hand side represent axial heat diffusion, convective conduction with the airstream and the heat of adsorption, respectively. For equation (4), the two terms on the left-hand side represent the transient storage and convection terms, whilst the terms on the right-hand side represent, the axial heat diffusion and the convective heat transfers with the adsorbent and outer tube walls, respectively. The different parameters in these equations represent the following: C_p (J/kg·K), λ_s (W/m·K) and T_s (K) are the adsorbent specific heat capacity, thermal conductivity, and temperature, respectively. h_{sg} (W/m^2·K) is the convective heat transfer coefficient between the airstream and the adsorbent. ρ_g (kg/m^3), C_g (J/kg·K), λ_g (W/m·K) and T_g (K) are the air density, specific heat capacity, thermal conductivity, and temperature, respectively. U_{wg} (W/m^2·K) is the overall heat transfer coefficient between the airstream and the ambient air of temperature T_{amb} (K). Σ_w (m^2/m^3) is the outer wall specific heat exchange area.

In order to solve the set of partial differential equations from (1) to (4), appropriate initial conditions were used. In addition, Danckwerts and pressure outlet boundary conditions were implemented at the bed's inlet and outlet [48], respectively as shown in Fig. 2(b). The Danckwerts boundary condition was used with dispersion models to ensure continuity at the inlet of the packed bed (node 1). Consequently, the developed model yields the outlet H_2O and CO_2 concentrations based on the following input parameters: physical parameters (bed geometry (H_b, D_b), adsorbent size (D_p)) and operating conditions (inlet air conditions and flowrate, and isotherms model).

3.2. Space model

The indoor air conditions of temperature, RH, CO_2, O_2 and formaldehyde concentrations are predicted using a transient model that assumes a perfectly homogenous mixed room air. In this study, the validated model of Yassine et al. [54] was adopted, which considers lumped energy and species' mass balances. The energy balance considers the external heat gains into the space from the building envelope ($\dot{Q}_{ext}(t)$) as well as from the internal sources ($\dot{Q}_{int}(t)$) such as occupants, lighting and electrical equipment as follows [55]:

$$\rho_a V_{space} C_{p,a}\frac{dT_{space}}{dt} = \dot{m}_{supp} C_{p,a}(T_{supp} - T_{space}) + \dot{Q}_{ext}(t) + \dot{Q}_{int}(t) \tag{5}$$

where ρ_a (kg/m^3) and $C_{p,a}$ (J/kg·K) are the air density and specific heat capacity of the indoor space of volume V_{space} (m^3) and temperature T_{space} (K). $\dot{m}_{supp}$ (kg/s) and T_{supp} (K) are the supply air flowrate and temperature, respectively.

Furthermore, the species' mass balance considers the mass exchanged by advection between the space supply and exhaust as well as the source/sink terms related to each species generation/consumption as follows [56]:

$$\rho_a V_{space}\frac{dy_i}{dt} = \dot{m}_{supp}(y_{i,supp} - y_i) \pm \dot{Y}_i \tag{6}$$

where y_i (kg/kg), $y_{i,supp}$ (kg/kg) are the species concentration in the indoor space air and the supply airstream, respectively. $\dot{Y}_i$ (kg/kg·s) is the generation rate (positive source terms) of either water vapor, CO_2 or formaldehyde and the consumption rate (negative sink term) of O_2.

3.3. Optimization methodology

The hourly performance of each system is evaluated based on its ability to meet the indoor space constraints at low operating cost. This is achieved by determining the optimal operating parameters of the ARS ($\dot{m}_{fa,ARS}$, $\dot{m}_{ta,ARS}$) and the conventional system ($\dot{m}_{fa,CS}$, β_{CS}) as a function of the ambient conditions and indoor occupancy. As stated in section 2, the total supply flowrate ($\dot{m}_{supp}$) to the space is dictated by the space load in Qatar [57]. It is thus determined on hourly basis by fixing the supply temperature to typical values obtained in vapor compression air-conditioning and is eliminated from the optimization search. The system operating cost consists of the required thermal (E_t) and electrical (E_e) energy. The thermal energy is the energy needed to heat the purge flowrate ($\dot{m}_{purge}$ (kg/s)) from the ambient air temperature (T_{amb} (K)) to the regeneration temperature (T_{reg} (K)):

$$E_t = \dot{m}_{reg} C_{p,a} (T_{reg} - T_{amb}) \tag{7}$$

The electrical energy powers the blower fans used to drive the air through the different system' subcomponents and supply to the space. It was calculated using the fan's affinity law that relates the fan power to its flowrate and the pressure drop [56]. The main contributor to the system's total pressure drop was the adsorption bed, where Ergun's equation, combining the viscous and kinetic pressure loss terms, was used as follows [48]:

$$\frac{\Delta P_b}{H_b} = \frac{600 \mu_g (1-\varepsilon_t)^2}{\pi \rho_g \varepsilon_t^3 D_p^2 D_b^2} \dot{m} + \frac{28(1-\varepsilon_t)}{\pi^2 \rho_g \varepsilon_t^3 D_p D_b^4} \dot{m}^2 \tag{8}$$

where μ_g (Pa·s) is the air viscosity. Additionally, the electrical energy of the vapor compression air-conditioner is determined from the cooling load by assuming a typical coefficient of performance of 3.2 [56].

The optimization problem of either systems consists of a multi-objective optimization with constraints. Accordingly, the genetic algorithm was used as the search tool to determine the optimal operating parameters of the conventional system and ARS. The genetic algorithm requires the definition of an objective function (J) that needs to be minimized. In this case, J was considered as the system operational cost. Since the system operation was subjected to the space thermal and IAQ constraints, the penalty function approach, introduced by Pierre [58], was adopted. In this approach, the objective function J consisted of the energy cost augmented by the penalty cost [59]. The energy terms reflect the monetary cost of the consumed thermal and electrical energy, while the penalty terms represent an additional cost is added to the objective function when the space thermal and IAQ constraints are violated [60]. Hence, the objective function is given by

$$J = \alpha_{RH} J_1 + \alpha_{IAQ} J_2 + \alpha_e E_e + \alpha_t E_t \tag{9}$$

$$J_1 = \left| \left(\frac{2 \times RH_{in} - RH_{min} - RH_{max}}{RH_{max} - RH_{min}} \right)^{2k} - 1 \right| \tag{9a}$$

$$J_2 = \exp\left(\frac{CO_{2,in}}{CO_{2,set}}\right) + \exp\left(\frac{O_{2,set}}{O_{2,in}}\right) + \exp\left(\frac{HCHO_{in}}{HCHO_{set}}\right) - 3 \tag{9b}$$

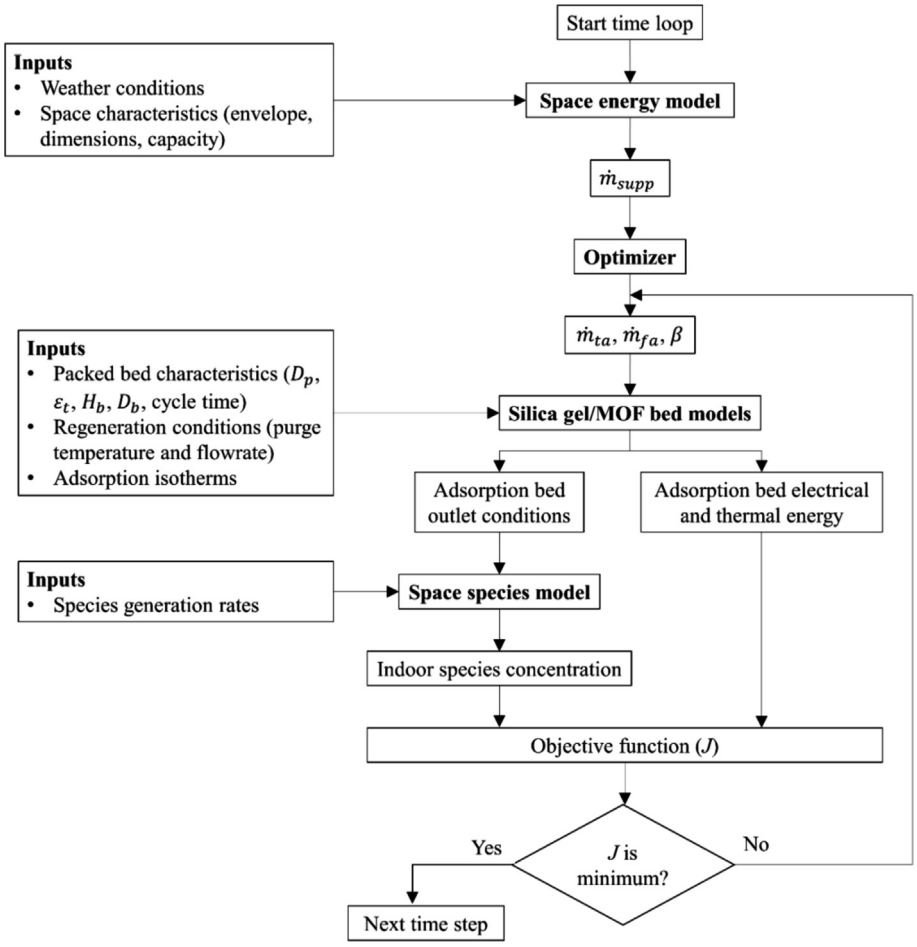

Fig. 3. Adopted numerical methodology to optimize the conventional system and ARS performance.

where RH_{in} (%), $CO_{2,in}$ (ppm) and $O_{2,in}$ (%) are the indoor RH, CO_2 and O_2 concentrations, respectively. RH_{max} (%), RH_{min} (%), $CO_{2,set}$ (ppm), $O_{2,set}$ (%) and $HCHO_{set}$ are the maximum and minimum indoor allowable RH levels, set-point CO_2, O_2 and formaldehyde concentrations, which are set to 65 %, 40 %, 1,000 ppm, 19.5% and 0.08 ppm respectively [61]. k (-) is a positive integer that forces the penalty term related to RH to attain values near zero within the allowable range $[RH_{min}, RH_{max}]$. This was achieved using a value of 2, which was found to be sufficient [59]. In addition, the IAQ constraints from their respective set-points were calculated using an exponential function [62]. For small deviations from the space constraints, J was considerably increased, which forced the solution to track the indoor set-points [60].

The different α 's are the weighting factors of the energy and penalty cost terms of the objective function, and were set to make the different terms of comparable order and to have equal significance in the evaluation of J [63]. Since the exponential formulation was adopted, each indoor condition was normalized with its corresponding set-point, which enabled α_{RH} and α_{IAQ} to be set to unity [62]. On the other hand, α_e and α_t represented the actual monetary cost of the electrical (0.013 USD/kWh_e) and thermal (0.133 USD/kWh_t) energy as adopted in Qatar [64–66]. Note that the heating of the purging airflows was supplied from the combustion of natural gas. This is due to its abundance on Qatar, its lower carbon emission compared to other fossil fuel, and to the simplicity of such heating system as compared to solar heating systems [67,68]. Finally, the population size of the genetic algorithm was set to 50 individuals with a maximum generation number of 100 [62]. The crossover fraction and function tolerance were set to 0.8 and 10^{-14}, respectively.

3.4. Numerical solution

Fig. 3 presents the optimization methodology adopted for the hybrid system integrating the adsorption beds models and the space models to evaluate the conventional system and ARS performance. At each time step, the **space energy model** yielded the cooling load using the weather data, space envelope and indoor occupancy. $\dot{m}_{supp}$ was then calculated and used in the optimizer that seeds the different operating parameters. The seeded parameters were used in the **silica gel/MOFs beds model** of both systems with the beds' geometries and adsorbent isotherms. The adsorption beds' outlet air conditions in terms of H_2O and CO_2 concentrations were used in the **space species model** to evaluate the indoor conditions of RH, CO_2 and O_2. Additionally, the adsorption beds' electrical and thermal energy were evaluated and added to the objective function along with the deviation of the indoor conditions from their set-points. The objective function was then evaluated, and the algorithm was repeated until an optimal solution was reached before moving to the next time step.

In order to numerically solve the adsorption bed and space models, the finite volume method was used with an implicit backward Euler scheme for transient terms in addition to the first order upwind and central difference schemes to discretize the convection and diffusion terms. A time-step independence test was performed and a time step of 10^{-3} s for the integrated model was found to yield accurate results at minimal computational time. The convergence criterion was set when the residuals, of any calculated parameters (temperatures and species concentrations), between two consecutive iterations were $<10^{-8}$.

4. Case study

The operating parameters of the systems depend on both the ambient conditions and indoor occupancy, which affect the energy consumption of the ambient air dehumidification and the needed fraction of recirculated air, respectively. Therefore, the dynamic performance of the proposed systems is evaluated for two case studies of a typical residential house and a classroom, representative of low and high occupancy spaces. The spaces are located in the hot and humid Qatari climate characterized by the large variability of the ambient air conditions. The ARS performance is evaluated over the entire hot season of Qatar (April through November). The weather data and solar radiation were based on typical meteorological year (TMY) data of Doha, Qatar [69]. Such database has been implemented in many previous studies for energy systems' modeling [70,71]. Fig. 4 presents the ambient air temperature (T_{amb}), RH (RH_{amb}) and the hourly horizontal solar radiation (S_h) for a representative day of each cooling month in Qatar.

4.1. Spaces characteristics

The typical residential house is assumed to be a two-story villa of 420 m^2 gross floor area [72] while the adopted classroom has a 50 m^2 floor area, both with south orientation and 3.5 m floor to ceiling height [73]. The building envelope of both case studies, presented in Table 1, follows the requirements imposed by the Qatar Construction Standard (QCS) 2014 and KAHRAMAA regulations [74]. It should be noted that these regulations specify an overall window-to-wall ratio of 20 % for the whole residential house. However, the maximum glazing area is restricted to the north façade [73]. The classroom is assumed to be exposed to the ambient conditions at the roof and the south façade. A window-to-wall ratio of 30 % of the south façade is adopted to maximize the natural daylight for the students' visual comfort [61]. Low transmittance glazing is used to reduce the heat gain due to direct solar irradiance and comply with KAHRAMAA regulations [74]. A maximum occupancy densities of 0.014 person/m^2 [57] and 0.66 person/m^2 [17] are considered for the residential house and classroom, respectively. Moreover, the maximum power density from lighting and electrical equipment are assumed to be 12 W/m^2 and 16 W/m^2 for the house and classroom, respectively [75]. The occupancy and electrical load schedule of both spaces are shown in Fig. 5. The metabolic activity of each person at 1.2 met is responsible for sensible and latent heat gains into the space as well as CO_2 and H_2O generation and O_2 consumption as summarized in Table 2 in addition to the total emission rate of formaldehyde (from furniture, paint).

4.2. Sizing methodology

The sizing of adsorption beds depends on the maximum adsorbate mass to be removed from the ventilation air stream of both systems ($\dot{m}_{fa,CS}$ and $\dot{m}_{ta,ARS}$). For the desiccant beds, the sizing is conducted at the peak latent load hour of each building during its occupied period, while for the carbon capture, the sizing is based on the highest CO_2 mass that needs to be removed during peak occupancy. The design flowrate ($\dot{m}_{des}$) is determined to yield a maximum indoor CO_2 levels of 1,000 ppm [17], since $\dot{m}_{fa,CS}$ and $\dot{m}_{ta,ARS}$ that circulate the packed beds are dictated by the indoor CO_2 generation.

The adsorbate mass depends primarily on the cycle (adsorption and desorption) time, the needed outlet humidity (ω_3 , Fig. 1) and CO_2 concentration at the bed outlet, the air flowrate to be treated with each system ($\dot{m}_{fa,CS}$, $\dot{m}_{ta,ARS}$) as well as the regeneration temperature and purge-to-feed flowrate ratio. In order to simplify the control strategy of the ventilation systems, an operation with a constant cycle time was chosen [78]. A fixed cycle time of 1800 s was thus adopted (within the typical cycle times) for both

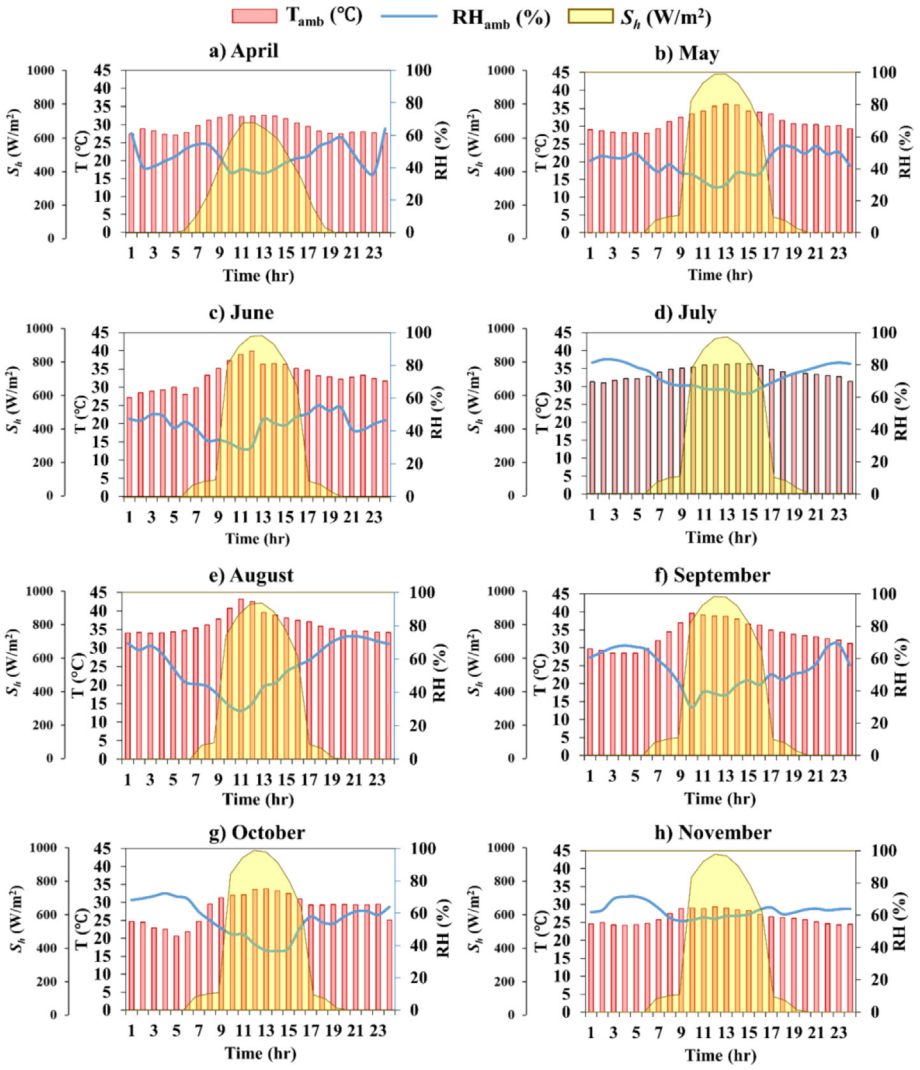

Fig. 4. Hourly variation of the ambient air temperature and RH and the horizontal solar radiation for a representative day of each month of the Qatari hot season [69].

Table 1
Building envelope for the adopted case studies [74].

Layer	*Composition*
Roof	250 mm concrete slab, with 75 mm polyurethane insulation U = 0.25 W/m^2·K
Floor	250 mm on-grade concrete slab
External walls	200 mm autoclaved aerated concrete U = 0.568 W/m^2 ·K
Internal partition	150 mm gypsum board
Windows	Double glazing low-E (e_2 = 0.04), Tint 6 mm, air 12 mm U = 1.64 W/m^2 ·K

systems' adsorption beds (i.e. the bed undergoes two cycles within one hour) [79]. The adsorption covers 70 % of the total cycle time while the remaining was dedicated for desorption [78]. The remaining design parameters are summarized in Table 3 for both systems. The needed ω_3 in the conventional system is related to the supply humidity to the space, which is typically around 7 g/kg [26]. On the other hand, ω_3 in the ARS is dictated by the need to eliminate the H_2O/CO_2 competitive adsorption on MOF-74-Mg, thus ω_3 must not exceed 4 g/kg as stated in section 2 [27]. The CO_2 outlet concentration depends on the extent of the MOFs' ability to reduce the CO_2 levels. In this regard, MOF-74-Mg has shown to be able to completely remove the CO_2 from an airstream. However, for practical reasons, the design outlet CO_2 concentration was set to 20 ppm in the ARS, as adopted by Cheng et al. [80]. This gives the advantage of reducing $\dot{m}_{ta,ARS}$ as compared to $\dot{m}_{fa,CS}$ while still meeting the indoor CO_2 levels. Finally, constant regeneration conditions were adopted for the different beds. The desorption temperature and flowrate were set to achieve 90 % regeneration of the beds within the allocated 540 s (i.e. 30 %) of the total cycle time. Finally, the beds are designed for minimum pressure drop by adopting a small length-to-diameter ratio, along with limiting the interstitial air velocity to a range between 1 and 3 m/s [78,81]. Using the above parameters ($\dot{m}_{des}$, cycle time, fluid velocity), the adsorption model is used to determine the packed beds dimensions (H_b , D_b) at the peak ambient temperature (highest adsorption temperature).

The dynamic performance of the adsorption beds depends on the adsorbents thermo-physical properties shown in Table 4. In addition, the dynamic model requires the equilibrium isotherms. Hence, the water/silica gel isotherms were modeled by the commonly used modified Freundlich model [83,84], whereas that of CO_2/MOF-74-Mg were modeled using the dual-site Langmuir

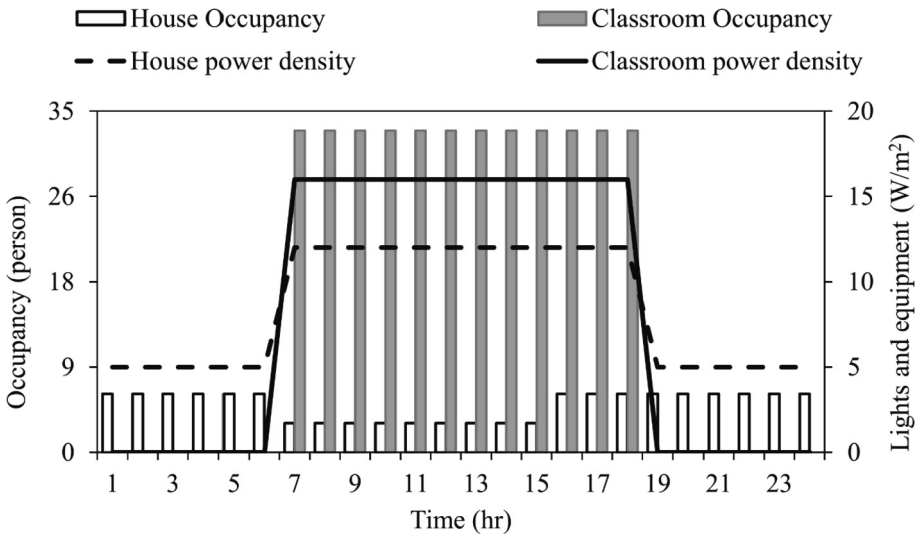

Fig. 5. Schedule of occupancy and load from lighting and electrical equipment for the residential house and classroom.

Table 2
Heat gains and species generation from indoor sources.

Parameter	*Value*	*Unit*	*Reference*
Sensible load	75.00	W/person	[75]
Latent Load	55.00	W/person	[75]
CO_2 generation	10.80	mg/s·person	[76]
H_2O generation	11.57	mg/s·person	[60]
O_2 consumption	9.92	mg/s·person	[40]
Formaldehyde generation	10.2[a]/55.5[b]	mg/h	[43,77]

a emission rate in classroom, [b] emission rate in residential houses

[85]. The isotherms' equations and their corresponding constants were presented by [84,86]. Note that the adsorbent was used in the form of beads of 1.7 mm [87], and were loosely packed into the beds formed of stainless steel cylinders insulated with 50 mm polyester core with aluminum jacketing [88].

5. Results and discussion

The current developed mathematical model of the packed bed was validated against published experimental and modeling data for both the adsorption bed of H_2O [88,89] and the adsorption bed of CO_2 [90,91] as presented in **Appendix A**. The validated model was used to size the conventional system and ARS following the strategy proposed in section 4.2, where the needed adsorbent mass as well as the corresponding packed bed dimensions (D_b , H_b) were determined for each adsorbent bed and for the two case studies of the residential house and the classroom as presented in **Appendix B**.

The validated models were integrated with a genetic algorithm to optimize the performance of these two systems for each case study following the methodology presented in Fig. 3. The obtained total energy consumptions of both systems were compared to determine the feasibility of the ARS through a LCCA.

5.1. Performance analysis of the conventional system and ARS

The performance of each system was optimized based on the methodology presented in Fig. 3 for the entire Qatari hot season. The simulation results are presented for three representative months of the low (May), moderate (June) and high (August) ambient conditions for both case studies of the classroom and residential house.

5.1.1. Case of high-occupancy buildings

Fig. 6 and Fig. 7 show the optimized operating parameters and the resulting electrical and thermal energy consumption, respectively for both the conventional system and ARS implemented in the classroom, representative of high-occupancy spaces.

For the conventional system implemented in the classroom during the month of May (Fig. 6(a)), the total supply flowrate $\dot{m}_{supp}$ depended on the cooling load, and varied between 0.47 kg/s and 0.6 kg/s, where the minimum was needed at the beginning of the occupied period (lowest load) whereas the maximum was required at peak load hour of *13:00 h*. Due to the low space load of this month and the high requirements on the fresh ambient air due to the high indoor occupancy, it can be seen that the supplied flowrate coincided with the needed amount of ambient air ($\dot{m}_{fa,CS} = \dot{m}_{supp}$). Moreover, it can be noticed that, due to the constant occupancy of the classroom, the required fresh air flowrate had small variation for controlling the indoor CO_2 levels. While in order to meet the indoor RH requirements, the supply air humidity was regulated with the bypass fraction β_{CS} on the desiccant bed. During the early and late hours of the day, the ambient humidity was elevated (Fig. 4(b)), increasing thus the dehumidifi-

Table 3
Design parameters for the H_2O and CO_2 adsorption beds of both systems.

System	*Design Parameter*				*References*
	Outlet humidity (g/kg)	*Outlet CO_2 (ppm)*	*Regeneration temperature (°C)*	*Purge-to-feed flowrate ratio (–)*	
Conventional	7	400	75	0.60	[35,78]
ARS	4	20	50	0.45	[27,82]

Table 4
Adsorbent thermos-physical properties.

Adsorbent	ΔH_i (kJ/kg)	ρ_s (kg/m^3)	$C_{p,s}$ (J/kg·K)	λ_s (W/m·K)	References
Silica gel	2,600	2,027	1,130	0.2	[35]
Mg-MOF-74	954*	921	900	0.3	[27,82,86]

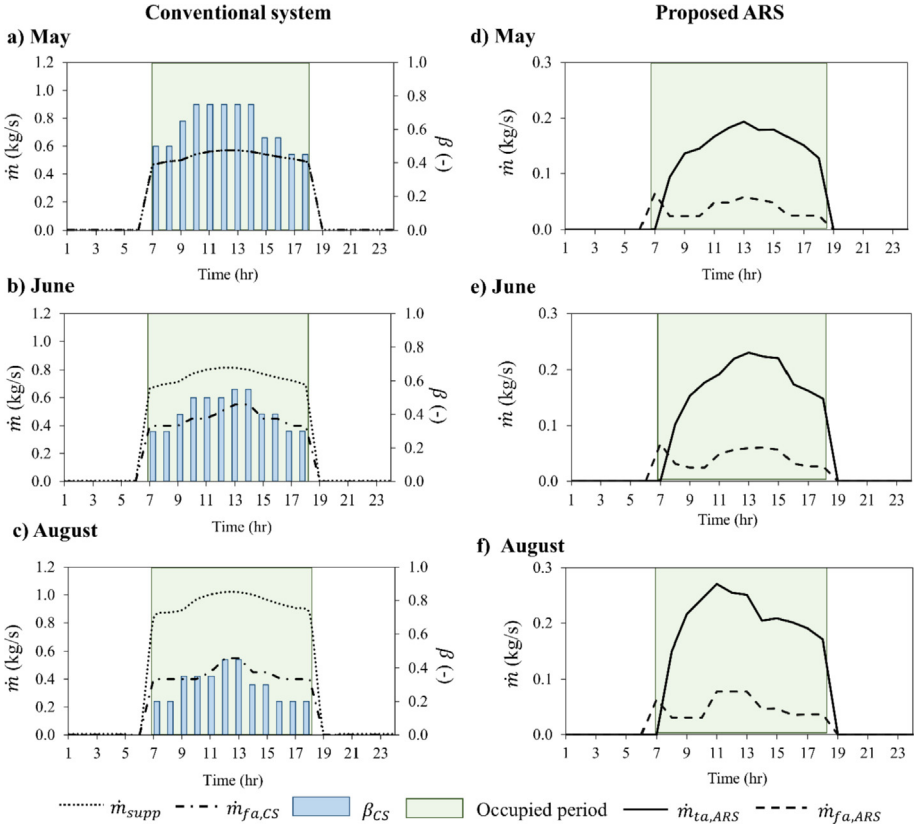

Fig. 6. The hourly variation of the optimal operating parameters for the conventional system during a) May, b) June and c) August and for the ARS during d) May, e) June and f) August for the classroom.

cation load, therefore, a low β_{CS} with an hourly average of 0.55 ± 0.05 was needed. As the ambient humidity decrease around noon, the hourly average of β_{CS} increased to 0.75 ± 0.1, due to the decrease in the latent load imposed on the adsorption bed (i.e. decrease in the ambient humidity) (Fig. 6(a)). The corresponding regeneration energy followed a similar trend as the dehumidification load: during the early and late hours of the day, the hourly needed E_t to regenerate the adsorbent varied around 2.82 ± 0.4 kWh_t and decreased to 1.42 ± 0.01 kWh_t during around noon hours (Fig. 7(a)). Similarly, the hourly needed electrical energy to operate the fans $E_{e,fan}$ was at its maximum of 1.04 ± 0.2 kWh_e when β_{CS} was at its minimum (i.e. higher flowrate that is treated in the adsorption bed) and decreased to 0.57 ± 0.01 kWh_e with the increase of β_{CS} . On the other hand, the electrical energy ($E_{e,coil}$) needed to sensibly cool $\dot{m}_{supp}$ increased from 5.5 kWh_e at the beginning of the day to 6.1 kWh_e at the peak load hour (*13:00 h*).

Similar trends for the operating parameters can be seen for the remaining months with low ambient conditions (April, October and November). During the month of June (Fig. 6(b)), the hourly average of $\dot{m}_{supp}$ varied around 0.71 ± 0.01 kg/s. However, the required ambient air flowrate $\dot{m}_{fa,CS}$ was reduced to 0.45 ± 0.05 kg/s as compared to May due to the increase in the ambient humidity. The maximum fresh flowrate of 0.55 kg/s was admitted to the space between *13:00 h – 14:00 h*, when the ambient humidity is low and the fresh air did not require excessive dehumidification. Furthermore, β_{CS} varied between 0.3, at the periods of high ambient humidity, to 0.55 at *13:00 h* when the ambient humidity was at its lowest levels (Fig. 4(c)). The resulting thermal and electrical energy followed similar patterns as those obtained in May but with higher levels. E_t and $E_{e,fan}$ varied around an hourly average 2.41 ± 0.8 kWh_t and 1.1 ± 0.32 kWh_e, respectively, where their minima were obtained around noon hours when the ambient humidity was low (Fig. 7(b)). On the other hand, $E_{e,coil}$ increased from 7.7 kWh_e to 8.1 kWh_e at the peak load hour (*13:00 h*). Similar performance was obtained for the month of September, characterized by moderate ambient conditions. During the peak month of August (Fig. 6(c)), $\dot{m}_{supp}$ increased from 0.8 kg/s (at *7:00 h*) to 1.1 kg/s (at *13:00 h*) to offset the peak classroom load, which typically reaches 210 W/m^2 for similar classroom in Qatar [92]. The needed fresh ambient air flowrate ($\dot{m}_{fa,CS}$) remained around 0.44 ± 0.05 kg/s since the fresh air intake is dictated by the need to regulate indoor CO_2 levels. Furthermore, due to the higher ambient humidity encountered in August, a lower β_{CS} of 0.3 ± 0.1 was needed to regulate the supply air humidity, where the maximum

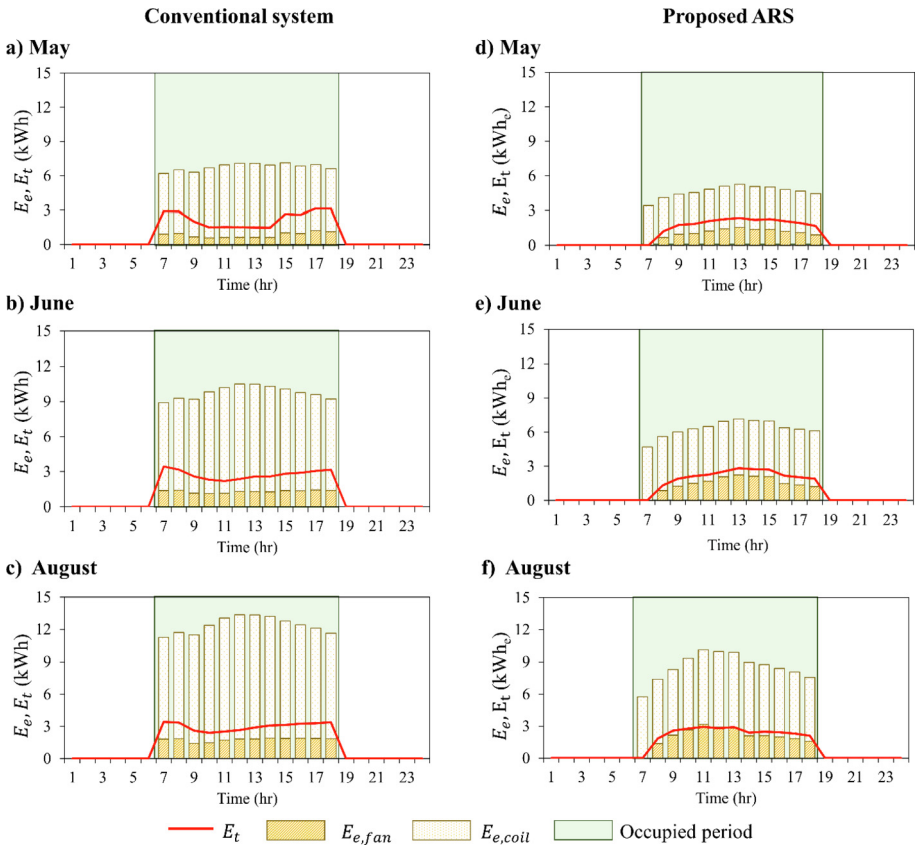

Fig. 7. The hourly variation of the conventional system' energy consumption during a) May, b) June and c) August and that of the ARS during d) May, e) June and f) August for the classroom.

was always needed at noon hours when ambient humidity was at its lowest values of the day. The resulting E_t , $E_{e,fan}$, $E_{e,coil}$ varied around 3.17 ± 1.0 kWh$_t$, 2.1 ± 0.72 kWh$_e$ and 10.6 ± 0.7 kWh$_e$, respectively (Fig. 7(c)). The electrical energy for the cooling coil of classroom located in Qatar during the month of August reached 3.8 MWh$_e$, in line with the findings of [92] Similar pattern for the operating parameters was obtained for the month of July, also characterized by high ambient conditions.

In the ARS, the supply air humidity ratio as well as the CO_2 concentration must be controlled, as opposed to the conventional system where only the air humidity was controlled. This was achieved by finding the hourly optimal operating parameters of this system which include the fresh ambient air flowrate ($\dot{m}_{fa,ARS}$) and the recirculated air flowrate that needed treatment ($\dot{m}_{ta,ARS}$). For both case studies, the supplied flowrate $\dot{m}_{supp}$ during all the simulated months were the same in the conventional system, since it depended on the spaces' cooling load.

During the month of May (Fig. 6(d)), the indoor CO_2 concentration decreased to the ambient levels of 400 ppm throughout the unoccupied nighttime period. This enabled the system to operate during the first occupied hour (*7:00 h*) with $\dot{m}_{ta,ARS}$ of zero, whereas $\dot{m}_{fa,ARS}$ of 0.06 kg/s was needed to maintain indoor O_2 and formaldehyde levels, while CO_2 concentration was also kept below 1,000 ppm. As the indoor CO_2 started to build up, $\dot{m}_{ta,ARS}$ increased to 0.16 ± 0.05 kg/s in order to maintain indoor CO_2 below 1,000 ppm (Fig. 7(d)). It should be noted that $\dot{m}_{ta,ARS}$ showed small variation since this flowrate depended primarily on the indoor CO_2 generation, which was constant throughout the occupied period. Moreover, $\dot{m}_{fa,ARS}$ varied around 0.04 ± 0.01 kg/s, which was the minimum required ambient flowrate needed to compensate the consumed indoor O_2. It should be noted that this flowrate was dictated by the consumption rate of O_2 due to the high occupancy, which enabled simultaneously to meet the formaldehyde levels of 0.08 ppm. Consequently, the resulting thermal (E_t) and fan energy ($E_{e,fan}$) followed the variation of $\dot{m}_{ta,ARS}$ increased from 1.24 kWh$_t$ and 0.67 kWh$_e$ to 2.38 kWh$_t$ and 1.57 kWh$_e$, respectively (Fig. 7(d)). In addition, the cooling energy needed for the coil ($E_{e,coil}$) varied between 3.4 kWh$_e$ and 3.7 kWh$_e$, which were considerably lower than that of the conventional system (Fig. 6(a)). This was attributed to two main reasons: i) the energy released from the adsorption was smaller than the case of conventional system due to the lower adsorbed water vapor volume and lower heat of CO_2 adsorption; ii) a higher recirculated air flowrate was used which increased the heat recovery and reduced the temperature of the airstream entering the cooling coil. Consequently, the ARS resulted in a reduction of 18.8 % and 30.4 % in the required thermal and electrical energy as compared to the conventional system, while maintaining the same thermal comfort and IAQ conditions. Similar trends can be seen for the operating parameters during the remaining months, where the resulting energy savings decreased as the ambient humidity decreased (during April, October and November). During the month of June (Fig. 6(e)), characterized by a higher ambient temperature, $\dot{m}_{ta,ARS}$ varied around 0.19 ± 0.06 kg/s with $\dot{m}_{fa,ARS}$ varying around 0.07 ± 0.03 kg/s. It can be seen that the needed ambient air is higher than the month of May, which was necessary to avoid increasing $\dot{m}_{ta,ARS}$ during peak ambient temperature. The resulting savings in E_t and E_e obtained by ARS compared to the conventional system reached 23.5 % and 31.3 % during this month, for the same indoor air conditions (Fig. 7(e)). During the peak month of August ((Fig. 6(f)), $\dot{m}_{ta,ARS}$ varied around 0.21 ± 0.07 kg/s, with the maximum of 0.27 kg/s was needed at *11:00 h*, when the ambient temperature reached its maximum of 44 °C

(Fig. 4). On the other hand, $\dot{m}_{ta,ARS}$ was reduced to 0.04 ± 0.03 kg/s due to the high humidity of August as compared to the previous months. The resulting thermal and electrical energy consumption were reduced by 27 % and 33.4 %, respectively (Fig. 7(f)), compared to the conventional system providing similar thermal comfort and air quality conditions inside the classroom. It can be seen that the reduction in the thermal and electrical energy achieved by the ARS reached its highest during the months with higher ambient humidity, while this reduction is reduced in the months with drier conditions. Over the entire hot season, the ARS was able to achieve a 91 % reduction in the fresh air intake, resulting in a reduction of 23 % and 31 % in the needed thermal and electrical energy as compared to the conventional system when they were implemented for the classroom.

It should be noted that the both $\dot{m}_{ta,ARS}$ and $\dot{m}_{fa,ARS}$ had small variation during the same day since they depended on the generation rate of CO_2 and consumption rate of O_2, respectively, which both where constant throughout the occupied period. Nonetheless, $\dot{m}_{ta,ARS}$ was increasing with the increase in the ambient conditions that affected the adsorption temperature of the MOF-74-Mg and reduced its capacity. As the ambient humidity increased from May to August, the entrained $\dot{m}_{fa,ARS}$ decreased (while remaining above the required minimum of 0.02 kg/s) to prevent increasing the supply humidity, and consequently the indoor RH.

5.1.2. Case of low-occupancy buildings

Fig. 8 shows the optimized operating parameters for both conventional system and ARS implemented in the residential house, representative of low-occupancy spaces. The resulting consumption of electrical and thermal energy of both systems are shown in Fig. 9.

For the residential house during the month of May (Fig. 8(a)), the hourly variation of the total supply flowrate ($\dot{m}_{supp}$) of the conventional system depended on cooling load. It varied between 0.7 kg/s during the early hours and 1.5 kg/s, needed to remove the space peak load (*17:00 h*). It can be seen that needed $\dot{m}_{supp}$ dropped to 1.1 kg/s at *13:00 h* due to the decrease in the indoor heat load (occupancy and electrical equipment). The ambient fresh air flowrate ($\dot{m}_{fa,CS}$) was entrained to regulate the indoor CO_2 levels, and thus depended on the occupancy levels. During the early (*1:00 h – 6:00 h*) and late (*16:00 h – 24:00 h*) hours of the day, $\dot{m}_{fa,CS}$ varied between 0.27 ± 0.05 kg/s, which dropped to 0.20 ± 0.02 kg/s between (*7:00 h – 15:00 h*) when the indoor occupancy decreased (Fig. 8(a)). Furthermore, in order to regulate the indoor RH, the supply air humidity was regulated by varying the bypass fraction (β_{CS}), where its hourly variation depended on the ambient humidity. During nighttime, the ambient humidity was relatively high (Fig. 4(b)), therefore, a low β_{CS} varying around 0.58 ± 0.1 was needed to offset the high latent load. However, as the ambient humidity decreased during daytime, β_{CS} increased to 0.93 ± 0.04 (Fig. 8(a)), where the ambient air could be introduced without dehumidification around noon hours. The resulting thermal energy (E_t) and electrical energy of the fans ($E_{t,fan}$) followed a trend similar to that of $\dot{m}_{fa,CS}$ and varied between 0 kWh_t and 0.47 kWh_e during daytime and 1.18 kWh_t and 1.17 kWh_e during nighttime (Fig. 9(a)). Additionally, the electrical energy for the cooling coil ($E_{e,coil}$) followed that of $\dot{m}_{supp}$ and varied between 8.43 kWh_e and 16.75 kWh_e, needed at peak load hour (Fig. 9(a)). For the remaining months, the hourly variation pf the operating parameters and running cost followed similar patterns as those of May.

During June (Fig. 8(b)), $\dot{m}_{supp}$ followed the variation of the space load and varied between 1.1 kg/s and 2.1 kg/s. $\dot{m}_{fa,CS}$ depended on the indoor occupancy and varied around 0.2 ± 0.05 kg/s during maximum occupancy and dropped to 0.16 ± 0.01 kg/s with the decrease in the occupancy (Fig. 8(b)). The decrease in the needed flowrate of ambient air was not proportional to that of the occupancy, which was due to lower humidity during the daytime hours. The lower ambient humidity enabled the increase in $\dot{m}_{fa,CS}$ to provide lower CO_2 levels without an added penalty on the system's operating cost. Furthermore, β_{CS} varied between 0.46 ± 0.16 during nighttime when the ambient humidity was elevated and the dehumidification load was higher and decreased to 0.7 ± 0.02 during nighttime with the decrease in the ambient humidity (Fig. 8(b)). It was clear that lower β_{CS} was needed during the month of June due to its higher humidity as compared to the month of May. The resulting E_t and $E_{e,fan}$ followed the variation of $\dot{m}_{fa,CS}$ and varied around 0.35 kWh_t and 0.84 kWh_e during daytime and 1.55 kWh_t and 1.78 kWh_e during nighttime. The cooling coil energy $E_{e,coil}$ followed the variation of the space load and $\dot{m}_{supp}$ and varied between 10.41 kWh_e and 23.94 kWh_e (Fig. 9(b)).

During the month of August (Fig. 8(c)), the peak month of the Qatari hot season and representative of high ambient conditions, the supply flowrate varied between 1.8 kg/s and 2.8 kg/s to offset the space peak load of 32 W/m^2, typically obtained in Qatari residence houses [72]. The ambient fresh ambient air intake decreased to its high humidity, and it varied between 0.13 ± 0.02 kg/s during maximum occupancy and dropped to 0.097 ± 0.01 kg/s when the occupancy decreased (Fig. 8(c)). To regulate the indoor humidity, the optimal β_{CS} varied around 0.15 ± 0.1 during the high humidity periods and increased to 0.41 ± 0.1 during nighttime. Lower $\dot{m}_{fa,CS}$ and β_{CS} were needed during the peak month of August as compared to the other months, which is attributed to its higher ambient humidity levels. Similarly to the other months, the corresponding E_t and $E_{e,fan}$ followed the variation of $\dot{m}_{fa,CS}$ and varied around 1 ± 0.4 kWh_t and 1.64 ± 0.45 kWh_e, respectively, while $E_{e,coil}$ followed similar trend as $\dot{m}_{supp}$ and varied between 14.4 kWh_e and 33.42 kWh_e (Fig. 9(c)).

The performance of the ARS for the residential house differed from that for the classroom, which was attributed to the occupancy schedule and level of indoor species generation. Since the house was occupied throughout the day, the ARS was always operated, where the optimal parameters ($\dot{m}_{fa,ARS}$ and $\dot{m}_{ta,ARS}$) were optimized to regulate both the humidity and CO_2 concentration in the supply airflow. For the month of May (Fig. 8(d)), $\dot{m}_{ta,ARS}$ and $\dot{m}_{fa,ARS}$ were varied around 0.07 ± 0.01 kg/s and 0.06 ± 0.005 kg/s to meet the IAQ constraints. It should be noted that in the case of the residential house, the ambient fresh air flowrate was dictated by the need to dilute the indoor formaldehyde levels, as opposed to the classroom, where the fresh air was needed to compensate the depleted O_2. As the occupancy dropped to its half and due to the low ambient humidity around noon hours, $\dot{m}_{fa,ARS}$ was increased to 0.09 ± 0.01 kg/s (Fig. 8(d)). This enabled to nullify the treated return air flowrate, since the ambient air flowrate was to dilute the different species without compromising the indoor RH. Consequently, the thermal energy E_t was negligible during these hours and increased to 1.2 kWh_t needed at the early hours of the day where the ARS was operated with the highest $\dot{m}_{ta,ARS}$. The fan electrical energy $E_{e,fan}$ varied between 0.66 kWh_e and 1.34 kWh_e and followed the variation in $\dot{m}_{ta,ARS}$, while that of the cooling coil $E_{e,coil}$ varied between 6 kWh_e and 13.43 kWh_e and followed the variation of $\dot{m}_{supp}$ (Fig. 9(d)). The resulting thermal and electrical energy consumption were reduced by 6.3 % and 24 % as compared to the conventional system. However, these savings were 70 % and 20 % lower than those obtained in the classroom. Therefore, when the conventional system was operated for residential house, low ambient flowrate were needed, which reduced its operating cost and in turn reduced the advantage of the ARS in low occupancy spaces.

During the month of June (Fig. 8(e)), the needed $\dot{m}_{ta,ARS}$ increased to around 0.09 kg/s to meet the needed CO_2 levels during maximum occupancy. The optimal $\dot{m}_{fa,ARS}$ was reduced to its mini-

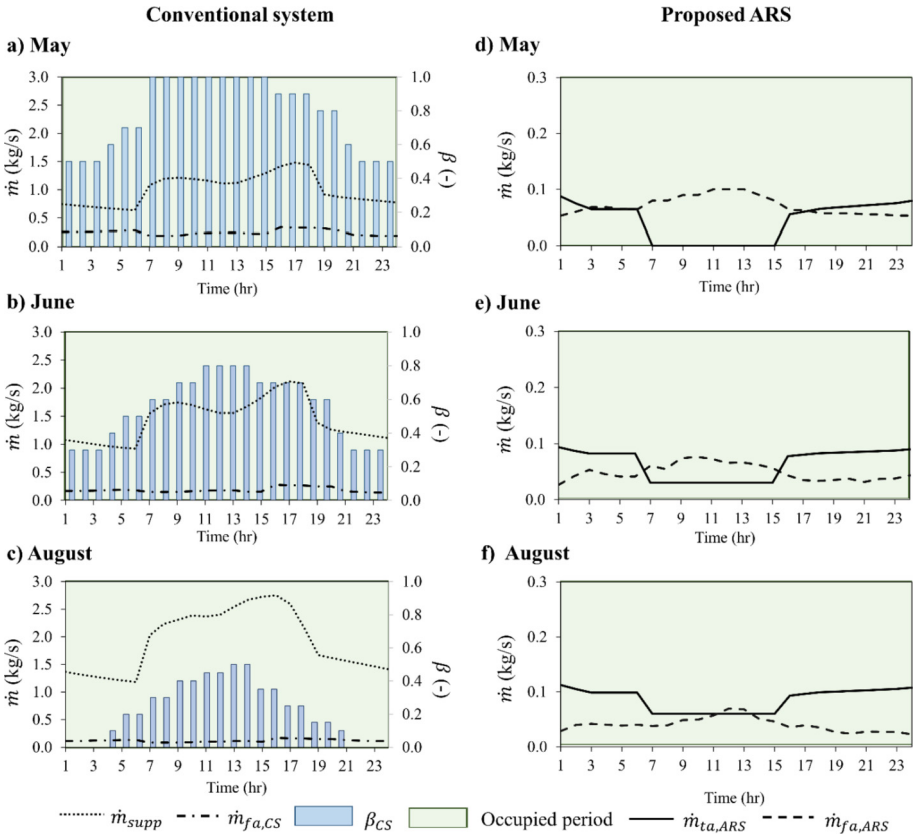

Fig. 8. The hourly variation of the optimal operating parameters for the conventional system during a) May, b) June and c) August and for the ARS during d) May, e) June and f) August for the residential house.

mum allowable limit of 0.04 kg/s necessary to regulate indoor formaldehyde levels, and consequently O_2 levels. During June, $\dot{m}_{fa,ARS}$ was lower than that obtained during the month of May, in order to avoid the increase in the indoor RH, which may arise from the higher ambient humidity during this month. However, similar to May, as the ambient humidity decreased around noon hours, $\dot{m}_{fa,ARS}$ increased to 0.065 kg/s needed to meet the IAQ requirements along with a decrease in $\dot{m}_{ta,ARS}$ to 0.03 kg/s (Fig. 8(e)), especially since the indoor occupancy decreased to its half. The corresponding E_t , $E_{e,fan}$ and $E_{e,coil}$ followed similar trends as those obtained during the month of May and varied around 0.84 ± 0.4 kWh_t, 1.33 ± 0.26 kWh_e and 11.72 ± 3 kWh_e, respectively (Fig. 9 (e)). Consequently, the ARS consumed 9.9 % and 25.11 % lower thermal and electrical energy as compared to the conventional system. Furthermore, as the ambient humidity reaches its highest levels during the peak month of August (Fig. 8(f)), the treated return air flowrate $\dot{m}_{ta,ARS}$ increased to 0.11 kg/s during the maximum occupancy hours in order to reduce the fresh air intake and avoid increasing the indoor RH. Consequently, $\dot{m}_{fa,ARS}$ was kept at its minimum of 0.033 kg/s to regulate the indoor formaldehyde levels below 0.08 ppm. (Fig. 8(f)) On the other hand, as the indoor occupancy decreased between *7:00 h – 13:00 h* and the ambient humidity decreased during the day, $\dot{m}_{ta,ARS}$ was reduced to 0.06 kg/s and $\dot{m}_{fa,ARS}$ was increased to 0.05 kg/s (Fig. 8(f)). The resulting E_t , $E_{e,fan}$ and $E_{e,coil}$ f varied around 1.0 ± 0.2 kWh_t, 1.81 ± 0.4 kWh_e and 15.64 ± 4.5 kWh_e, respectively (Fig. 9(f)). Accordingly, the ARS offered 10% and 26.5 % lower thermal and electrical energy consumption as compared to the conventional system in high ambient conditions. Over the entire hot season, the ARS yielded a reduction of 71 % in the fresh air intake, which led to savings of 7 % and 25 % in the required thermal and electrical energy compared to the conventional system. As it was the case of the classroom, the savings in the operating cost resulting from the implementation of the ARS were reduced in the months of low ambient humidity and reached their maximum during the peak month of August. Moreover, these savings are considerably lower than those obtained in the classroom, especially the savings in the thermal energy. This is attributed to the lower ambient air flowrate that needed dehumidification in the residential house, which resulted in lower regeneration energy and reduced the savings when compared to the ARS.

5.2. Economic performance and LCCA

From the above presented results, it can be seen that both conventional system and ARS were able to provide similar indoor air conditions that met the occupant's thermal comfort and IAQ requirement, whereas the ARS offered a lower operating cost as compared to the conventional system, especially in the months with high ambient humidity. Nonetheless, due to the need for an additional adsorbent for carbon capture, as well as the higher cost of the MOFs as compared to the conventional adsorbents, the capital cost of the ARS was higher. Consequently, an economic analysis was conducted through a LCCA in order to determine the payback period of the proposed ARS for both residential house and classroom case studies. The life-cycle cost (*LCC* (USD)) of each system was determined using equation (10):

$$LCC = C_{ini} + \sum_{j=1}^{N} \frac{C_j^O + C_j^M}{(1+a)^j} = C_{ini} + \sum_{j=1}^{N} \frac{C_j^E + C_j^T + C_j^M}{(1+a)^j} \quad (10)$$

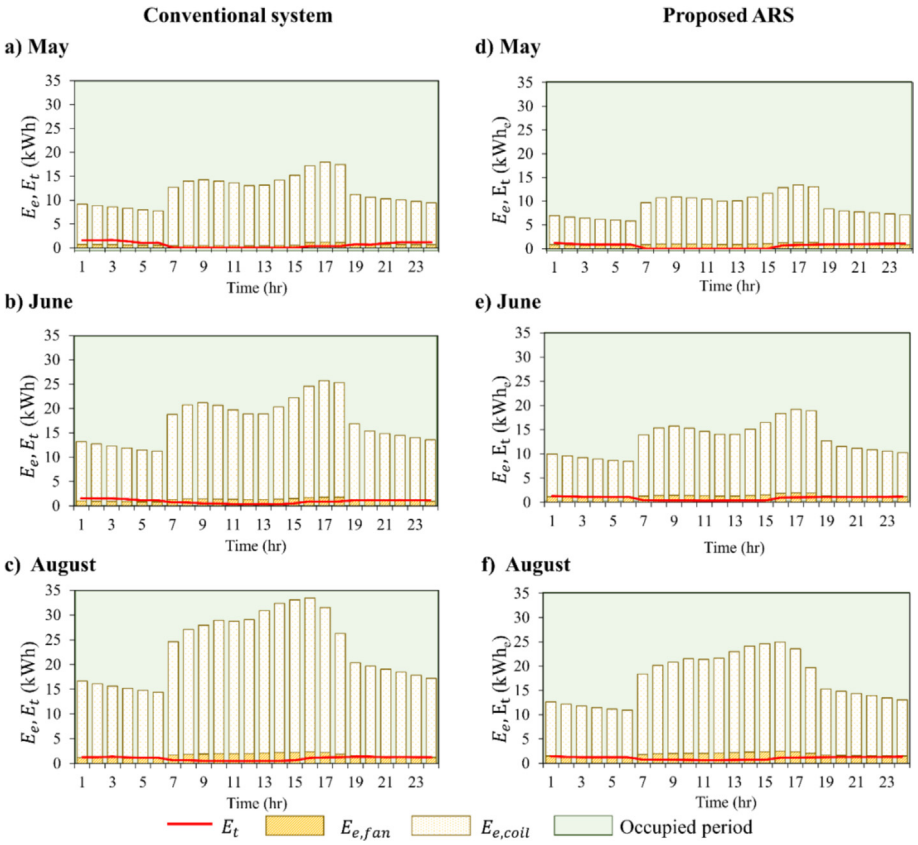

Fig. 9. The hourly variation of the conventional system' energy consumption during a) May, b) June and c) August and that of the ARS during d) May, e) June and f) August for the classroom.

where C_{ini} (USD) is the initial investment cost, C_j^O (USD) and C_j^M (USD) are the yearly operating and maintenance costs, respectively. The operating cost takes into consideration the cost of consumed thermal (C_j^T (USD)) and electrical (C_j^E (USD)) energy. N is the holding period of the system and a is the discount rate, which are adopted in this work as 30 years [93], with a typical discount rate value of 8 % [57]. An initial cost of 18 USD/kg silica gel [57] and 48.52 USD/kg of MOF-74-Mg [94] were used to determine the initial investments of the systems. Furthermore, the electrical energy and thermal energy (from natural gas) costs in Qatar were 0.013 USD/kWh$_e$ and 0.133 USD/kWh$_t$, respectively [64–66]. As for C_j^M , it included the maintenance of the adsorption beds, fans and vapor compression air-conditioner, which was assumed to be 2 % of each system's C_{ini} [93]. Fig. 10 shows the resulting *LCC* for the proposed ARS as compared to that of the conventional systems for both the residential house and classroom. It can be seen that the ARS achieved 30 % and 24 % reduction with a payback period of years 5 and 2 years for the classroom and residential house, respectively as compared to the conventional system. It can be seen that the small ARS size in the residential house resulted in a shorter payback period as compared to the classroom, even though the energy savings were higher in the latter case.

5.3. Limitations and applicability

The proposed ARS system is designed for climates that are predominantly hot and humid. However, its feasibility has been demonstrated in dry ambient conditions as well, where it showed significant reduction in the operating cost. The proposed system has some limitations, especially for residential buildings where there are some restrictions due to its required large footprint (adsorption beds, heat exchangers and regeneration system), which necessitates large technical areas that are not always available. Solar energy can be used for the regeneration of the adsorbents, instead of the combustion of natural gas, which increases the system sustainability. However, energy storage systems are then required to provide the needed thermal energy during nighttime.

Furthermore, the study only considered one type of adsorbent (MOF-74-Mg) for carbon capture that was able to meet the indoor space requirements while providing a reduction in the operating cost. Nonetheless, more advanced adsorbent from the MOF family can be more suitable candidates for this application such as Nb-OFFIVE-1-Ni [31] and the SIFSIX-n-M family [27,95,96]. Such MOFs are not commercially available yet, however, they present better stability and higher capacity for CO_2 adsorption even in humid conditions. Their use enables the treatment of the return air for CO_2 and H_2O capture simultaneously within a single adsorption bed, which is the subject of future studies. Additionally, the payback period of the ARS compared to the conventional system depends largely on the initial cost of the system, mainly that of the MOF. In this study, the cost of MOF-74-Mg has been adopted based on the conventional solvothermal synthesis, nonetheless, other methods have proven to provide lower adsorbent cost, and consequently, shorter payback period.

6. Conclusion

Conventional HVAC systems employ ambient fresh air for the rejuvenation of enclosed spaces and the abatement of indoor pol-

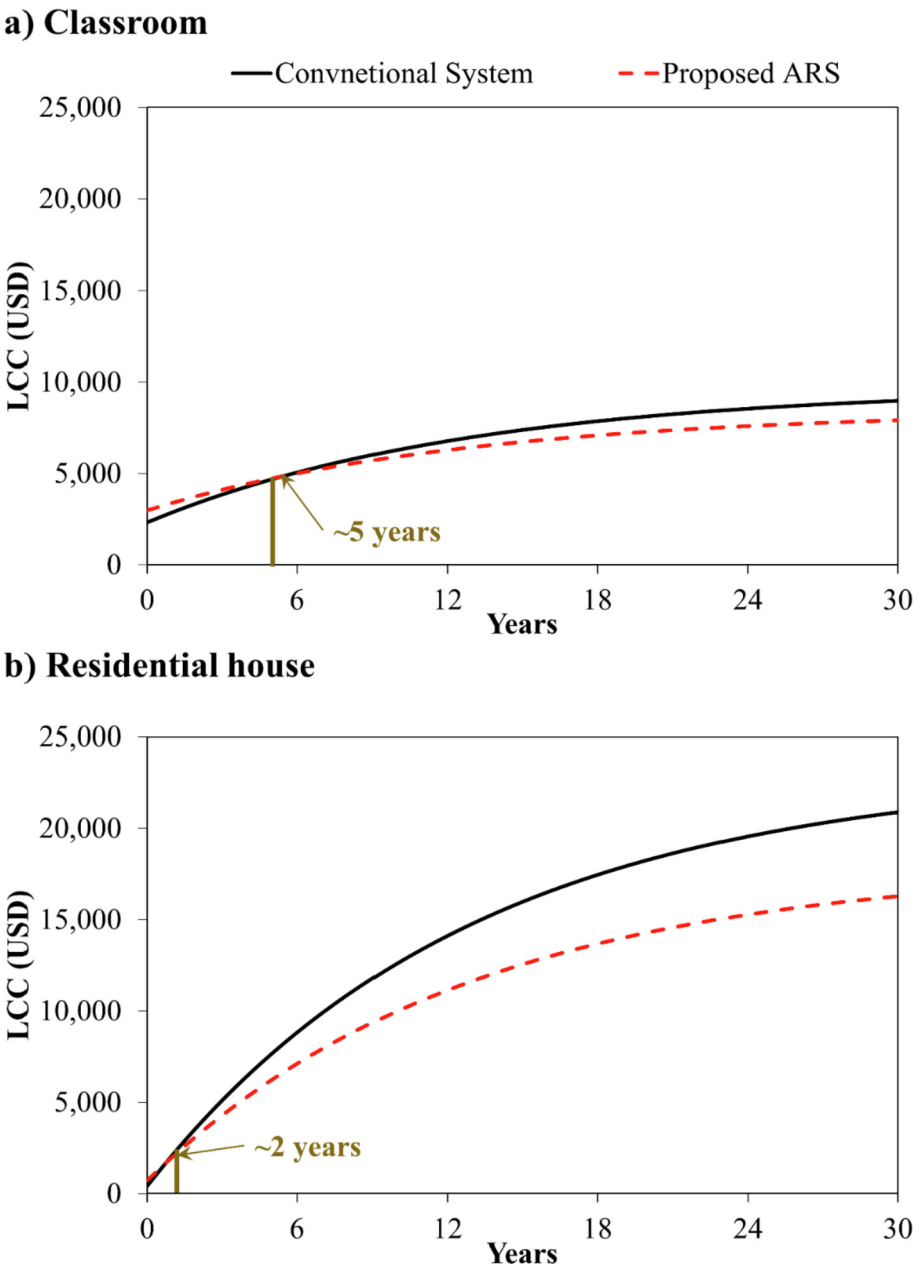

Fig. 10. *LCC* of the proposed ARS as compared to the conventional system for a) classroom, and b) residential house.

lutants. However, such techniques are energy intensive due to the need for excessive hygrothermal conditioning of the ambient air to maintain the occupants' thermal comfort. Therefore, there is a need to propose an HVAC system that provides the IAQ requirements at reduced fresh air intake. Accordingly, adsorption-based air treatment techniques are adopted in this work, to regulate the indoor CO_2 and H_2O concentrations. Such systems considerably reduce the intake of fresh ambient air, which is reflected in the reduction of the building electrical power, in addition to making use of low-grade thermal energy sources. Hence, the feasibility of the complete HVAC system integrated with carbon capture from indoor air (referred to by ARS) is investigated vis-à-vis the conventional system based on the desiccant dehumidification of the ambient air. The hybrid systems were sized, and their performance was optimized for two case studies of a classroom and residential house located in the predominantly hot and humid climate of Qatar. For this reason, mathematical models were developed for the integrated systems and validated with the published data in the literature.

The performance of the systems was then simulated and compared over the hot season of the Qatari climate (April to November) for each case study. The hourly variation of the indoor air conditions showed that the ARS was able to meet the thermal comfort and IAQ constraints throughout the entire hot season. A comparative economic analysis showed that, over the entire hot season:

- The implementation of ARS achieved higher reduction in the operating cost during the months with higher ambient humidity and for the spaces with higher indoor occupancy.
- The ARS was able to achieve 91 % reduction in the fresh air intake, leading to 30 % lower operating cost with a payback period of 6 years compared to the conventional system for high occupancy buildings.

- The ARS required 71 % lower ambient air, which achieved 24 % lower operating cost with a payback period of 2 years compared to the conventional system for low occupancy buildings.

Declaration of Competing Interest

The authors declare that they have no known competing financial interests or personal relationships that could have appeared to influence the work reported in this paper.

Acknowledgments

The authors would like to acknowledge the financial support of the American University of Beirut – Masri Institute of Energy and Natural Resources. The findings achieved herein are solely the responsibility of the authors. The collaborative research was made possible by the award (QUEX-CENG-ASPIRE-11/12-7) from ASPIRE Zone Foundation, Doha, Qatar.

Appendix A. Model validation

The accuracy of the developed models is critical for the validity of the findings. Accordingly, the model of adsorption beds was validated with the published data for both H_2O and CO_2 capture.

For the dehumidification bed, the model was validated against the experimental data of Swardsuk et al. [89]. Using the modified Freundlich isotherms, the same bed geometry (H_b = 1 m, D_b = 0.2 m), an adsorption time of 1800 s, an inlet air flowrate of 20 L/s at temperature and RH of 30 ℃, 53 %, respectively. It was found that the outlet temperature and humidity were in agreement with the experimental data as shown in Fig. A.1**(a)**, with maximum error on the outlet temperature and humidity was 6.1 % and 5.93 %, respectively. The water adsorption model was further validated against the experimental results of Baghapour et al. [88]. For the same bed (H_b = 0.2 m, D_b = 0.1016 m), adsorption time (1800 s) and inlet air conditions (air velocity of 0.3 m/s, temperature of 33 °C and RH of 56 %), the maximum discrepancies on the outlet temperature and humidity were found to be 2.0 % and 6.4 %, respectively.

For the carbon capture bed, the model was validated with the numerical model of Qasem et al. [86], that adopted the same isotherms model for MOF-74-Mg as this work. For the same bed (H_b= 0.07 m, D_b = 0.004 m) and inlet conditions (volumetric air flowrate of 20 mL/min, 0.1/0.9 CO_2/N_2 concentration, temperature of 27 ℃, RH of 10%), the error on the CO_2 retention time was 5.6 %, whereas the maximum error on the outlet air temperature and CO_2 concentration were 8.4 % and 9.6 %, respectively. Moreover, the model is validated with the numerical results of Ben-Mansour and Qasem [90] for the same bed geometry as before and for inlet dry airstream with CO_2/N_2 concentration of 0.2/0.8. The errors on

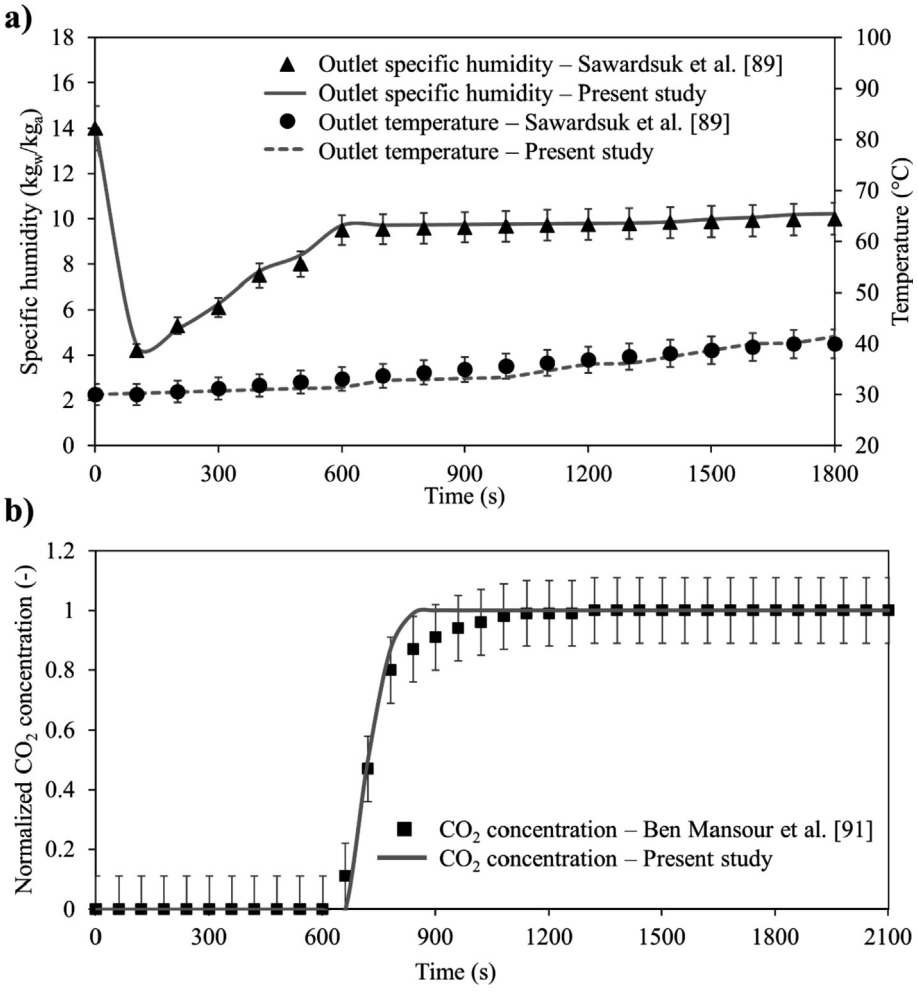

Fig. A.1. Validation of the outlet air conditions for a) the desiccant bed and b) for the carbon capture bed.

Table B.1
Adsorption beds sizing for the conventional system and ARS for both case studies.

Space	*Residential house*		*Classroom*	
System	*Conventional*	*ARS*	*Conventional*	*ARS*
$\dot{m}_{des}$ *(kg/s)*	*0.064*	*0.040*	*0.397*	*0.224*
Dehumidification bed				
Silica gel mass (kg)	11.0	4.0	64.0	15.0
H_b *(m)*	0.20	0.10	0.30	0.20
D_b *(m)*	0.30	0.25	0.60	0.35
Carbon capture bed				
MOF-74-Mg mass (kg)	–	3.5	–	25.0
H_b *(m)*	–	0.10	–	0.25
D_b *(m)*	–	0.35	–	0.60

the retention time, outlet temperature and CO_2 concentration are 6.2 %, 7.3 % and 8.9 %, respectively. Further validation of the mathematical model for CO_2 capture was conducted with the experimental results of Ben-Mansour et al. [91] for the bed geometry (H_b= 0.2 m, D_b = 0.009 m) and inlet conditions (dry air flowrate of 10 mL/min, 0.2/0.9 CO_2/N_2 concentration, temperature of 24 ℃). The outlet CO_2 concentration (normalized with respect to the inlet concentration) was in good agreement with the experimental data as shown in Fig. A.1**(b)** with a maximum error on the retention time and outlet CO_2 concentration of 5.7 %, and 9.5 %, respectively.

Appendix B. System sizing

The proper operation of the systems depends on its sizing. Following the strategy proposed in section 4.2, the different adsorption beds were sized by determining the needed adsorbents mass as well as the corresponding packed bed dimensions (D_b, H_b) as presented in Table B.1. The mass flowrates that were used for the design ($\dot{m}_{des}$ in Table B.1) corresponded to the flowrates needed to maintain a CO_2 concentration of 1,000 ppm. This flowrate depended on the supply CO_2 concatenation (400 ppm for the conventional system and 20 ppm for the ARS). In addition, the sizing of the dehumidification bed of the conventional system was conducted using $\dot{m}_{des}$ at the peak latent load of the Qatari hot season, which falls in the month of August.

References

[1] N.E. Klepeis et al., The National Human Activity Pattern Survey (NHAPS): a resource for assessing exposure to environmental pollutants, J. Eposure Sci. Environ. Epidemiol. 11 (3) (2001) 231–252.
[2] R. Pitarma, G. Marques, B.R. Ferreira, Monitoring indoor air quality for enhanced occupational health, J. Med. Syst. 41 (2) (2017) 1–8.
[3] J. Ding, C.W. Yu, S.-J. Cao, HVAC systems for environmental control to minimize the COVID-19 infection, Indoor Built Environ. 29 (9) (2020) 1195–1201.
[4] A. Kusiak, M. Li, H. Zheng, Virtual models of indoor-air-quality sensors, Appl. Energy 87 (6) (2010) 2087–2094.
[5] W. Li, S. Wang, A multi-agent based distributed approach for optimal control of multi-zone ventilation systems considering indoor air quality and energy use, Appl. Energy 275 (2020) 115371.
[6] M.J. Colligan, The psychological effects of indoor air pollution, Bull. N. Y. Acad. Med. 57 (10) (1981) 1014.
[7] M.D. Nembhard, D.J. Burton, J.M. Cohen, Ventilation use in nonmedical settings during COVID-19: Cleaning protocol, maintenance, and recommendations, Toxicol. Ind. Health 36 (9) (2020) 644–653.
[8] B.N. Young, W.O. Benka-Coker, Z.D. Weller, S. Oliver, J.W. Schaeffer, S. Magzamen, How does absenteeism impact the link between school's indoor environmental quality and student performance?, Build. Environ. (2021) 108053.
[9] A. Dounis, M. Bruant, G. Guarracino, P. Michel, M. Santamouris, Indoor air-quality control by a fuzzy-reasoning machine in naturally ventilated buildings, Appl. Energy 54 (1) (1996) 11–28.
[10] U. Satish et al., Is CO2 an Indoor Pollutant? Direct Effects of Low-to-Moderate CO2 Concentrations on Human Decision-Making Performance, Environ. Health Perspect. 120 (12) (2012) 1671–1677, https://doi.org/10.1289/ehp.1104789.
[11] G.J. Berbari, Fresh air treatment in hot and humid climates, ASHRAE J. 40 (10) (1998) 64.
[12] U. S. E. I. Administration. "Commercial Building Energy Consumption Survey, Consumption and Expenditures." (accessed..
[13] L. Pérez-Lombard, J. Ortiz, C. Pout, A review on buildings energy consumption information, Energy Build. 40 (3) (2008) 394–398, https://doi.org/10.1016/j.enbuild.2007.03.007.
[14] D. Jani, M. Mishra, P. Sahoo, Performance analysis of hybrid solid desiccant–vapor compression air conditioning system in hot and humid weather of India, Build. Serv. Eng. Res. Technol. 37 (5) (2016) 523–538.
[15] A. Baayoun et al., Emission inventory of key sources of air pollution in Lebanon, Atmos. Environ. 215 (2019), https://doi.org/10.1016/j.atmosenv.2019.116871 116871.
[16] J. Hansen, M. Sato, R. Ruedy, A. Lacis, V. Oinas, Global warming in the twenty-first century: an alternative scenario, Proc. Natl. Acad. Sci. 97 (18) (2000) 9875–9880.
[17] ANSI/ASHRAE Standard 62.1-2010. Ventilation for acceptable indoor air quality, ASHRAE, 2010..
[18] G. Marques, C.R. Ferreira, R. Pitarma, Indoor air quality assessment using a CO 2 monitoring system based on internet of things, J. Med. Syst. 43 (3) (2019) 1–10.
[19] A. Franco, E. Schito, Definition of optimal ventilation rates for balancing comfort and energy use in indoor spaces using CO2 concentration data, Buildings 10 (8) (2020) 135.
[20] J. Wilcox, Carbon Capture, Springer Science & Business Media, 2012.
[21] C. Major, B. Sollami, K. Kammermeyer, Carbon dioxide removal from air by adsorbents, Ind. Eng. Chem. Process Des. Dev. 4 (3) (1965) 327–333.
[22] H. Furukawa, K. E. Cordova, M. O'Keeffe, and O. M. Yaghi, "The chemistry and applications of metal-organic frameworks," *Science,* vol. 341, no. 6149, p. 1230444, 2013. [Online]. Available: https://science.sciencemag.org/content/sci/341/6149/1230444.full.pdf..
[23] E.T. Gall, C. Sonat, W.W. Nazaroff, C. Unluer, Investigating CO2 removal by Ca- and Mg-based sorbents with application to indoor air treatment, Build. Environ. 110 (2016) 161–172.
[24] R. Zhao et al., Thermodynamic exploration of temperature vacuum swing adsorption for direct air capture of carbon dioxide in buildings, Energy Convers. Manage. 183 (2019) 418–426.
[25] T.S. Lee, J.H. Cho, S.H. Chi, Carbon dioxide removal using carbon monolith as electric swing adsorption to improve indoor air quality, Build. Environ. 92 (2015) 209–221.
[26] A. Sinha, H. Thakkar, F. Rezaei, Y. Kawajiri, M.J. Realff, Direct Air Capture of CO2 in Enclosed Environments: Design under Uncertainty and Techno-Economic Analysis, in: M.R. Eden, M.G. Ierapetritou, G.P. Towler (Eds.), Computer Aided Chemical Engineering, Elsevier, 2018, pp. 2179–2184.
[27] S. Mukherjee *et al.*, "Trace CO2 capture by an ultramicroporous physisorbent with low water affinity," Science Advances, 5(11), p. eaax9171, 2019..
[28] T. Ghanbari, F. Abnisa, W.M.A.W. Daud, A review on production of metal organic frameworks (MOF) for CO2 adsorption, Sci. Total Environ. 707 (2020) 135090.
[29] J. Park et al., Metal–organic framework adsorbent for practical capture of trace carbon dioxide, ACS Appl. Mater. Interfaces 12 (45) (2020) 50534–50540.
[30] Y. Belmabkhout, V. Guillerm, M. Eddaoudi, Low concentration CO2 capture using physical adsorbents: are metal–organic frameworks becoming the new benchmark materials?, Chem. Eng. J. 296 (2016) 386–397.
[31] P.M. Bhatt et al., A fine-tuned fluorinated MOF addresses the needs for trace CO2 removal and air capture using physisorption, J. Am. Chem. Soc. 138 (29) (2016) 9301–9307.
[32] R.K. Motkuri, J. Liu, C.A. Fernandez, S.K. Nune, P. Thallapally, B.P. McGrail, Metal organic frameworks-synthesis and applications, Ind. Catal. Sep. (2014) 61–103.
[33] R. Ben-Mansour et al., Carbon capture by physical adsorption: materials, experimental investigations and numerical modeling and simulations–a review, Appl. Energy 161 (2016) 225–255.
[34] G. Li, P. Xiao, P.A. Webley, J. Zhang, R. Singh, Competition of CO2/H2O in adsorption based CO2 capture, Energy Procedia 1 (1) (2009) 1123–1130.

[35] X. Wang, W. Zimmermann, K. Ng, A. Chakraboty, J. Keller, Investigation on the isotherm of silica gel+ water systems, J. Therm. Anal. Calorim. 76 (2) (2004) 659–669.
[36] P. Silva, S.M. Vilela, J.P. Tomé, F.A.A. Paz, Multifunctional metal–organic frameworks: from academia to industrial applications, Chem. Soc. Rev. 44 (19) (2015) 6774–6803.
[37] J. Wang et al., Direct capture of low-concentration CO2 on mesoporous carbon-supported solid amine adsorbents at ambient temperature, Ind. Eng. Chem. Res. 54 (19) (2015) 5319–5327.
[38] ANSI/ASHRAE Standard 55-2017: Thermal Environmental Conditions for Human Occupancy, ASHRAE, 2017..
[39] A. Luengas, A. Barona, C. Hort, G. Gallastegui, V. Platel, A. Elias, A review of indoor air treatment technologies, Rev. Environ. Sci. Bio/Technol. 14 (3) (2015) 499–522.
[40] M.K. Kim, L. Baldini, H. Leibundgut, J.A. Wurzbacher, N. Piatkowski, A novel ventilation strategy with CO2 capture device and energy saving in buildings, Energy Build. 87 (2015/01/01/ 2015,) 134–141, https://doi.org/10.1016/j.enbuild.2014.11.017.
[41] N. R. Council, "Formaldehyde-an assessment of its health effects," 1980..
[42] L. Zhang, Formaldehyde: Exposure, Toxicity and Health Effects, Royal Society of Chemistry, 2018.
[43] T. Salthammer, S. Mentese, R. Marutzky, Formaldehyde in the indoor environment, Chem. Rev. 110 (4) (2010) 2536–2572.
[44] T.G. Myers, F. Font, M.G. Hennessy, Mathematical modelling of carbon capture in a packed column by adsorption, Appl. Energy 278 (2020) 115565.
[45] S. Li et al., Mathematical modeling and numerical investigation of carbon capture by adsorption: literature review and case study, Appl. Energy 221 (2018) 437–449.
[46] T.L. Dantas et al., Carbon dioxide–nitrogen separation through adsorption on activated carbon in a fixed bed, Chem. Eng. J. 169 (1–3) (2011) 11–19.
[47] K.S. Hwang, W.K. Lee, The adsorption and desorption breakthrough behavior of carbon monoxide and carbon dioxide on activated carbon. Effect of total pressure and pressure-dependent mass transfer coefficients, Sep. Sci. Technol. 29 (14) (1994) 1857–1891.
[48] M.S. Shafeeyan, W.M.A.W. Daud, A. Shamiri, A review of mathematical modeling of fixed-bed columns for carbon dioxide adsorption, Chem. Eng. Res. Des. 92 (5) (2014) 961–988.
[49] İ. Solmuş, D.A.S. Rees, C. Yamalı, D. Baker, B. Kaftanoğlu, Numerical investigation of coupled heat and mass transfer inside the adsorbent bed of an adsorption cooling unit, Int. J. Refrig 35 (3) (2012) 652–662.
[50] C. Tien, Introduction to Adsorption: Basics, Analysis, and Applications, Elsevier, 2018.
[51] İ. Solmuş, D.A.S. Rees, C. Yamalı, D. Baker, A two-energy equation model for dynamic heat and mass transfer in an adsorbent bed using silica gel/water pair, Int. J. Heat Mass Transf. 55 (19–20) (2012) 5275–5288.
[52] M. Clausse, J. Bonjour, F. Meunier, Adsorption of gas mixtures in TSA adsorbers under various heat removal conditions, Chem. Eng. Sci. 59 (17) (2004) 3657–3670.
[53] M. Clausse, J. Merel, F. Meunier, Numerical parametric study on CO2 capture by indirect thermal swing adsorption, Int. J. Greenhouse Gas Control 5 (5) (2011) 1206–1213.
[54] B. Yassine, K. Ghali, N. Ghaddar, I. Srour, G. Chehab, A numerical modeling approach to evaluate energy-efficient mechanical ventilation strategies, Energy Build. 55 (2012) 618–630, https://doi.org/10.1016/j.enbuild.2012.08.042.
[55] E. Katramiz, N. Ghaddar, K. Ghali, "Daytime radiative cooling: To what extent it enhances office cooling system performance in comparison to night cooling in semi-arid climate?, J. Build. Eng. 28 (2020), https://doi.org/10.1016/j.jobe.2019.101020 101020.
[56] J.P. Harrouz, K. Ghali, N. Ghaddar, Integrated solar–Windcatcher with dew-point indirect evaporative cooler for classrooms, Appl. Therm. Eng. 188 (2021) 116654.
[57] E. Katramiz, H. Al Jebaei, S. Alotaibi, W. Chakroun, N. Ghaddar, K. Ghali, Sustainable cooling system for Kuwait hot climate combining diurnal radiative cooling and indirect evaporative cooling system, Energy 213 (2020), https://doi.org/10.1016/j.energy.2020.119045 119045.
[58] D.A. Pierre, Optimization Theory with Applications, Courier Corporation, 1986.
[59] C. Jin et al., Engineering-oriented dynamic optimal control of a greenhouse environment using an improved genetic algorithm with engineering constraint rules, Comput. Electron. Agric. 177 (2020) 105698.
[60] M. Mossolly, K. Ghali, N. Ghaddar, Optimal control strategy for a multi-zone air conditioning system using a genetic algorithm, Energy 34 (1) (2009) 58–66.
[61] ASHRAE, *ASHRAE Handbook- 2017 Fundamentals*. American Society of Heating, Refrigerating and Air-Conditioning Engineers, Inc..
[62] A. Keblawi, N. Ghaddar, K. Ghali, Model-based optimal supervisory control of chilled ceiling displacement ventilation system, Energy Build. 43 (6) (2011) 1359–1370.
[63] S. Wang, X. Jin, Model-based optimal control of VAV air-conditioning system using genetic algorithm, Build. Environ. 35 (6) (2000) 471–487.
[64] "Water and electricity tariffs for productive farms in Qatar." https://www.km.qa/CustomerService/Pages/Tariff.aspx (accessed..
[65] "Woqod - FAQs." http://www.woqod.com/EN/AboutUs/Pages/FAQs.aspx (accessed..
[66] M. El Hourani, K. Ghali, N. Ghaddar, Effective desiccant dehumidification system with two-stage evaporative cooling for hot and humid climates, Energy Build. 68 (2014) 329–338.
[67] J. Dargin, Qatar's natural gas: the foreign-policy driver, Middle East Policy 14 (3) (2007) 136.
[68] E. Delarue, W. D'haeseleer, Greenhouse gas emission reduction by means of fuel switching in electricity generation: addressing the potentials, Energy Convers. Manage. 49 (4) (2008) 843–853.
[69] U. S. D. o. Energy. "EnergyPlus: Typical meteorological year." https://energyplus.net/weather (accessed..
[70] D.K. Al Assaad et al., A sustainable localised air distribution system for enhancing thermal environment and indoor air quality of poultry house for semiarid region, Biosyst. Eng. 203 (2021) 70–92.
[71] M. Saghafifar, M. Gadalla, Performance assessment of integrated PV/T and solid desiccant air-conditioning systems for cooling buildings using Maisotsenko cooling cycle, Sol. Energy 127 (2016) 79–95.
[72] O. Alrawi, I.S. Bayram, S.G. Al-Ghamdi, M. Koc, High-resolution household load profiling and evaluation of rooftop pv systems in selected houses in qatar, Energies 12 (20) (2019) 3876.
[73] Y. Alhorr, "GSAS ECOLEAF.".
[74] (2014). *Qatar Construction Standard 2014*..
[75] A. S. ASHRAE, "Standard 90.1-2004, Energy standard for buildings except low rise residential buildings," *American Society of Heating, Refrigerating and Air-Conditioning Engineers, Inc*, 2004..
[76] A. Persily, L. de Jonge, Carbon dioxide generation rates for building occupants, Indoor Air 27 (5) (2017) 868–879.
[77] T. Salthammer, Formaldehyde sources, formaldehyde concentrations and air exchange rates in European housings, Build. Environ. 150 (2019) 219–232.
[78] A.A. Pesaran, A.F. Mills, Moisture transport in silica gel packed beds—I. Theoretical study, Int. J. Heat Mass Transf. 30 (6) (1987) 1037–1049.
[79] L. Chai et al., Ventilation rates in large commercial layer hen houses with two-year continuous monitoring, Br. Poult. Sci. 53 (1) (2012) 19–31.
[80] H.-H. Cheng, C.-S. Tan, Removal of CO2 from indoor air by alkanolamine in a rotating packed bed, Sep. Purif. Technol. 82 (2011) 156–166.
[81] J.-Y. San, G.-D. Jiang, Modeling and testing of a silica gel packed-bed system, Int. J. Heat Mass Transf. 37 (8) (1994) 1173–1179.
[82] A. Kumar et al., Direct air capture of CO2 by physisorbent materials, Angew. Chem. Int. Ed. 54 (48) (2015) 14372–14377.
[83] A. Sakoda, M. Suzuki, Fundamental study on solar powered adsorption cooling system, J. Chem. Eng. Jpn. 17 (1) (1984) 52–57.
[84] H. Hassan, A. Mohamad, Y. Alyousef, H. Al-Ansary, A review on the equations of state for the working pairs used in adsorption cooling systems, Renew. Sustain. Energy Rev. 45 (2015) 600–609.
[85] J.A. Mason, K. Sumida, Z.R. Herm, R. Krishna, J.R. Long, Evaluating metal–organic frameworks for post-combustion carbon dioxide capture via temperature swing adsorption, Energy Environ. Sci. 4 (8) (2011) 3030–3040.
[86] N.A. Qasem, R. Ben-Mansour, Adsorption breakthrough and cycling stability of carbon dioxide separation from CO2/N2/H2O mixture under ambient conditions using 13X and Mg-MOF-74, Appl. Energy 230 (2018) 1093–1107.
[87] A. Zouaoui, L. Zili-Ghedira, S.B. Nasrallah, Solid desiccant solar air conditioning unit in Tunisia: numerical study, Int. J. Refrig 74 (2017) 662–681.
[88] B. Baghapour, M. Rouhani, and M. Bahrami, "EXPERIMENTAL DESIGN AND PERFORMANCE ANALYSIS OF A DESICCANT DEHUMIDIFICATION COLUMN UNDER CYCLIC OPERATING CONDITIONS.".
[89] P. Sawardsuk, J. S. Jongyingcharoen, and E. Cheevitsopon, "Experimental investigation of air characteristics during dehumidification in the multilayer desiccant bed column system," in: MATEC Web of Conferences, 2018, vol. 192: EDP Sciences, p. 03012..
[90] R. Ben-Mansour, N.A. Qasem, An efficient temperature swing adsorption (TSA) process for separating CO2 from CO2/N2 mixture using Mg-MOF-74, Energy Convers. Manage. 156 (2018) 10–24.
[91] R. Ben-Mansour, N.A. Qasem, M.A. Antar, Carbon dioxide adsorption separation from dry and humid CO2/N2 mixture, Comput. Chem. Eng. 117 (2018) 221–235.
[92] M. R. Bible, "Modeling building energy use and hvac efficiency improvements in extreme hot and humid regions," Texas A & M University, 2011..
[93] J.P. Harrouz, E. Katramiz, K. Ghali, D. Ouahrani, N. Ghaddar, Comparative analysis of sustainable desiccant – evaporative based ventilation systems for a typical Qatari poultry house, Energy Convers. Manage. 245 (2021), https://doi.org/10.1016/j.enconman.2021.114556 114556.
[94] D. DeSantis, J.A. Mason, B.D. James, C. Houchins, J.R. Long, M. Veenstra, Techno-economic analysis of metal–organic frameworks for hydrogen and natural gas storage, Energy Fuels 31 (2) (2017) 2024–2032.
[95] K.A. Forrest et al., Investigating CO2 sorption in SIFSIX-3-M (M= Fe Co, Ni, Cu, Zn) through computational studies, Cryst. Growth Des. 19 (7) (2019) 3732–3743.
[96] O. Shekhah et al., Made-to-order metal-organic frameworks for trace carbon dioxide removal and air capture, Nat. Commun. 5 (1) (2014) 1–7.